Contact: Chip Guard, National Weather Service-Guam
Office: (671) 472-0946
Cell: (671) 777-244

FOR IMMEDIATE RELEASE

National Weather Service in Guam and the University of Guam Release Typhoon Soudelor Wind Assessment for Saipan, CNMI

Contact: Mark A. Lander, University of Guam
Office: (671) 735-2695

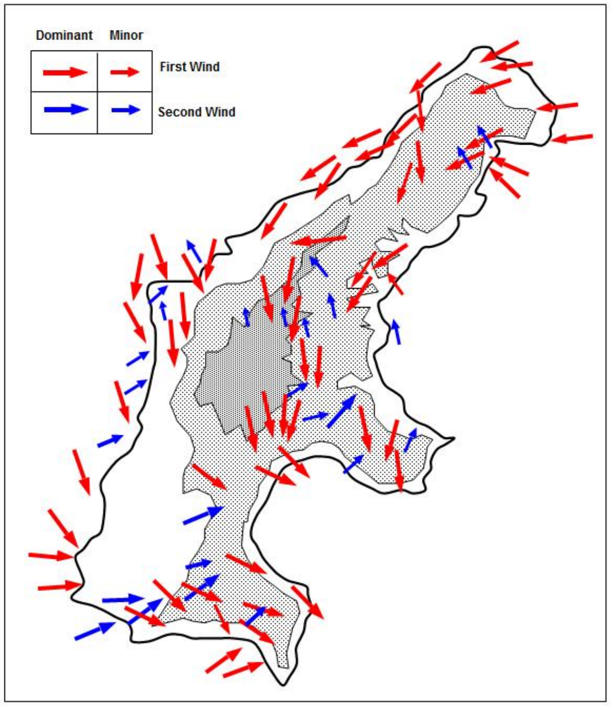

Contact: Chip Guard, National Weather Service-Guam **SUPPLEMENTAL RELEASE**

Office: (671) 472-0946
Cell: (671) 777-2447

National Weather Service in Guam and the University of Guam Supplemental Release Typhoon Soudelor Wind Assessment for Saipan, CNMI

This document is a supplement to the press release of 20 August 2015 made by the Soudelor on Saipan assessment team of Charles P. Guard and Mark A. Lander. In the earlier assessment, Soudelor was ranked as a high Category 3 tropical cyclone, with peak over-water wind speed of 110 kts with gusts to 130 kts (127 mph with gusts to 150 mph). As noted in the first press release, some of the damage on Saipan was consistent with even stronger gusts to at-or-above the Category 4 threshold of 115kt with gusts to 140 kt (130 mph with gusts to 160 mph). After considering the hundreds of damage pictures obtained on-site by the team and a careful analysis of the other factors relating to typhoon intensity, such as the measurements of the minimum central pressure and the characteristics of Soudelor's eye on satellite imagery, the team has now raised it's estimate of Soudelor equivalent over-water intensity to the 115 kt (130 mph) sustained wind threshold of a Category 4 tropical cyclone. The typical peak gust associated with a tropical cyclone of this intensity is 140 kt (162 mph). Gusts of this magnitude are capable of causing the type of extensive damage seen on portions of central Saipan. Not every part of the island experienced these peak gusts. The north and south ends of the island were spared the worst because those locations were not located under the inner portion of the eyewall. The central west coast of the island had some of the most impressive wind damage, with hundreds of healthy mature ironwood trees uprooted or snapped at the trunk. Patches and swaths of heavier wind damage are readily explained by turbulent wind flow across complex terrain. The treefall pattern, however, was surprisingly coherent, and nicely delimits the path of the small typhoon across the mid-section of the island. The First Wind was dominant at most locations, with the Second Wind having a minor signal in most areas, which was a likely the result of the great extent of treefall in the First Wind. The presence of some trees in close proximity felled in opposite directions was thought by some to be evidence of tornadoes, but most, if not all, of the treefall pattern is consistent with the large-scale cyclonic swirling flow of the typhoon itself.

The reason for this supplemental release is to offer a slight change of the assessed intensity and to provide a single reference value. In the original press release, the typhoon over-water intensity was assessed a bit lower. Patches of damage that seemed to be outliers slightly in excess of the assigned typhoon wind speed range were attributed to gusts enhanced by terrain or perhaps even small-scale features within the typhoon eyewall itself. Particularly after carefully studying the treefall pattern, the assessment team felt that the large-scale swirling wind of the typhoon with a sustained wind and peak gust of a single magnitude (e.g., 115 kt ; G 140 kt) would be an appropriate metric from which one could account for all the observed effects of the typhoon. The patches of heavier damage are now viewed as areas where, for reasons of complex terrain and exposure, the peak over water gust of 140 kt was experienced in full force.

On the following pages, some useful images and charts are included. The original press release is appended.

Visible Satellite imagery captures the tiny "pinhole" eye of Soudelor that formed prior to its passage over Saipan, and continued to be present as it tracked across and past the island.

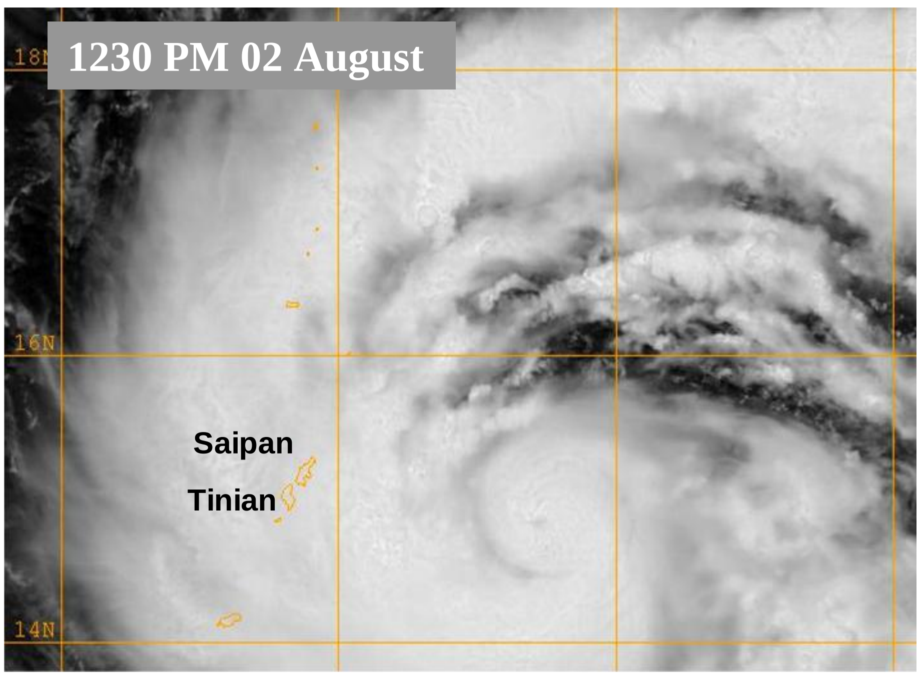

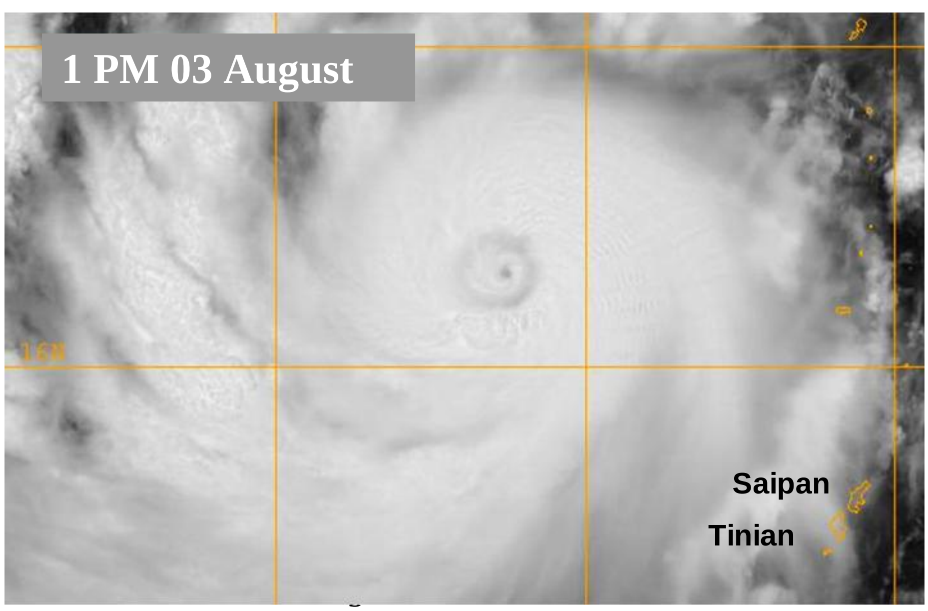

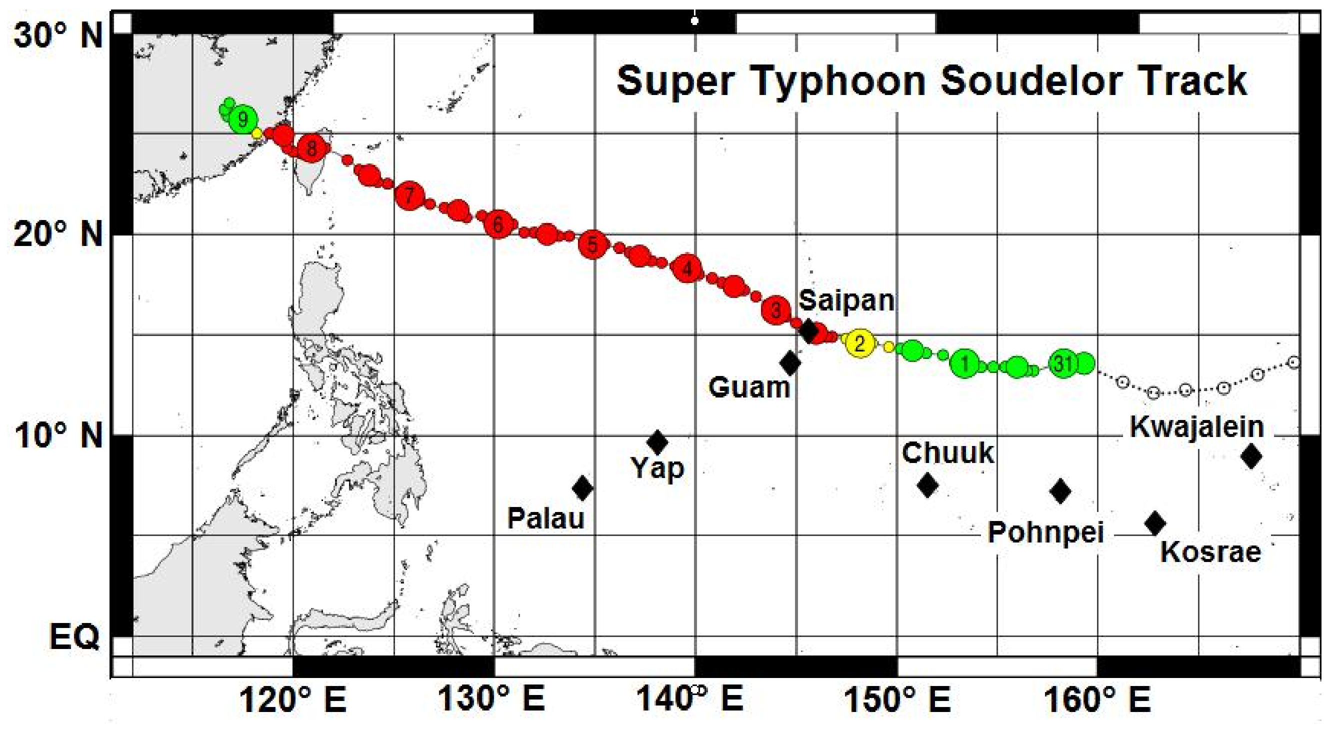

Typhoon Soudelor track across the western North Pacfic.

Radar Composite Reflectivity

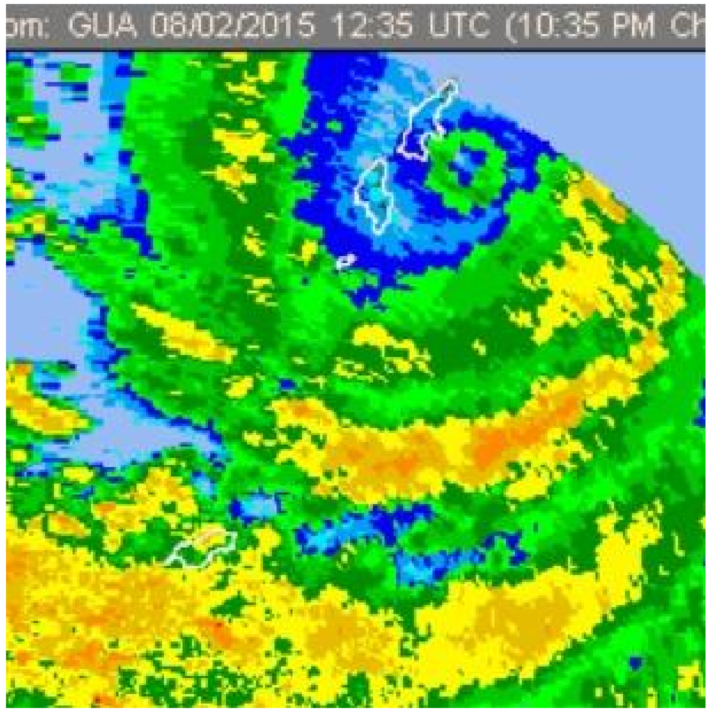

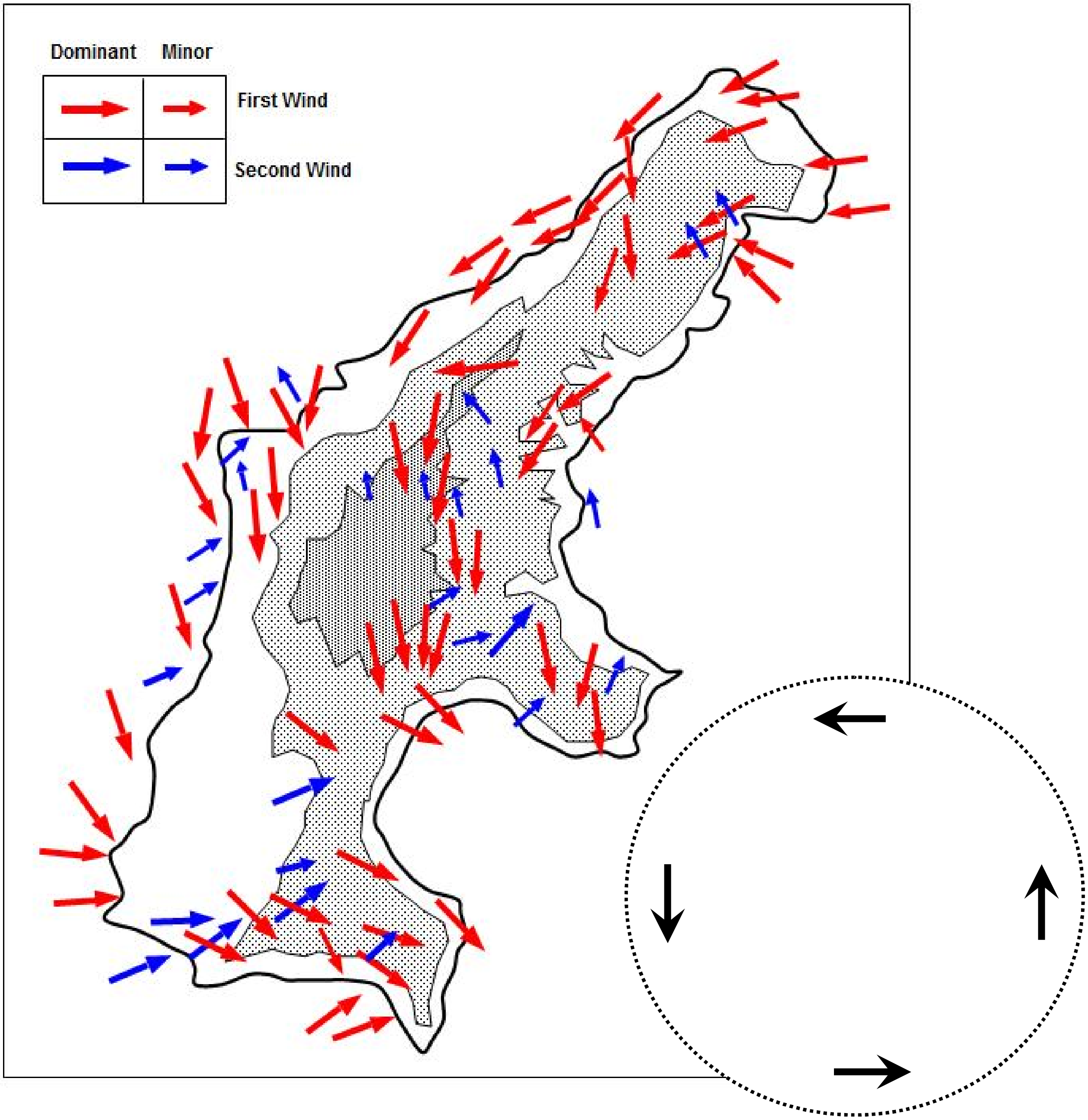

A map of the treefall pattern on Saipan caused by Typhoon Soudelor. The typhoon spins counterclockwise, so as the eye passes across the island, the winds are first from a northerly direction (red arrows), then after the eye passes, the winds switch direction and have a southerly component (blue arrows). Most of the observed treefall was from the First Wind. There were fewer trees blown over by the Second Wind, primarily because there were so many trees blown over by the First Wind (almost 100% in some places) that there was little left for the Second Wind. Many eyewitnesses perceived that the First Wind was stronger than the Second Wind. Stippled areas show high ground: outer stippled area > 50 m, inner stippled area > 200 m.

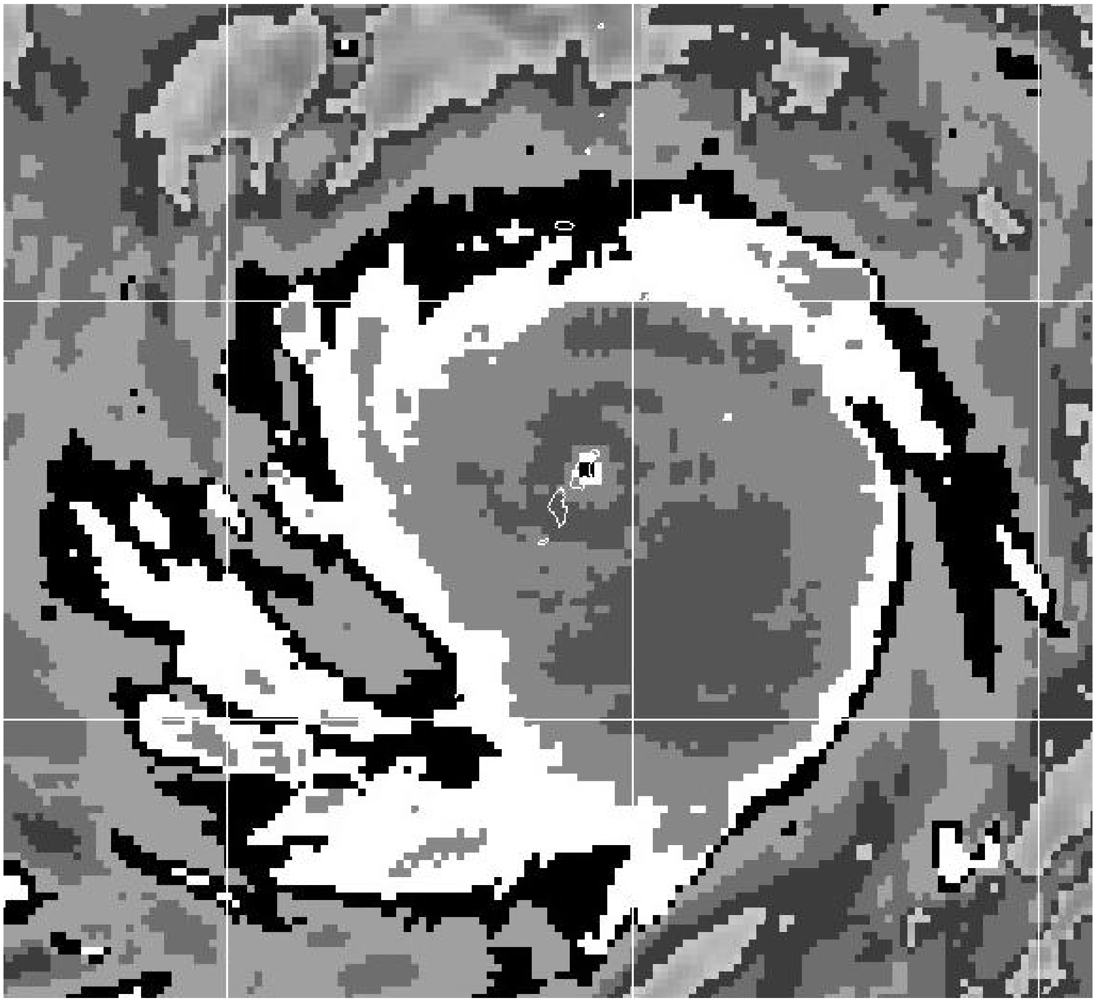

Enhanced IR (BD Curve)
1301 UTC 02 August 2015 (0101 AM 03 August Local)

Dvorak Analysis: Ring = CMG = T6.5
Eye Adjust B inside CMG = -0.5
Data T Number = **T 6.0**

Enhanced Infrared imagery of Soudelor at the time that its eye was directly over Saipan. A sequence of false gray shades are applied to the infrared brightness to indicate the cloud-top temperature. From the temperature data, the intensity of the typhoon can be derived using Dvorak's technique for estimating typhoon intensity from it characteristics on the satellite imagery. In this image, the intensity is derived to be **T 6.0**, which is equivalent to 115 kt one-minute sustained wind with peak gusts to 140 kt.

APPENDIX: UNFINISHED Full Report of Typhoon Soudelor on Saipan.

METEOROLOGICAL ASSESSMENT
FOR TYPHOON SOUDELOR IN SAIPAN, CNMI

By

The National Oceanic and Atmospheric Administration (NOAA) National Weather Service (NWS) Meteorological Assessment Team for
Typhoon Soudelor

Charles 'Chip' Guard, NWS Forecast Office Guam
Mark A. Lander, University of Guam

August 2015

1. Background: Typhoon Soudelor passed directly over the island of Saipan with a ferocity that stunned island residents. The level of damage, especially to vegetation, wooden homes, and utility poles was severe. The storm had a very unique structure when it hit Saipan late on the night of 02 August 2015: its core was of midget dimensions (Fig. 1), with the calm region of the eye only 4 miles across at ground level. In fact, the entire core of the typhoon – eye and eyewall convective ring – tracked within the 12 miles of separation between the north and south bounds of the island. The landfall intensity of Soudelor was much higher than anticipated in the last forecasts that most island residents probably heard before the near-midnight rampage of the storm. The forecast intensity shortfall (real and perceived), the severity of the damage (enough to fuel a widespread belief of island residents that tornadoes had accompanied the typhoon), and the very unusual structure of the typhoon prompted a quick request and authorization for this metrological assessment. On behalf of the Pacific Region Headquarters of the National Weather Service, and working around limited flights to the island, the complete loss of base-load power and municipal water service, and the general post-typhoon chaos, the meteorological assessment team members Charles P. "Chip" Guard and Mark A. Lander arrived on Saipan one week after the typhoon event to conduct a thorough damage assessment. What is contained herein is the team's meteorological assessment for Typhoon Soudelor in Saipan, including a determination of the landfall intensity and of the factors contributing to the jaw-dropping level of damage.

The island of Saipan has not had a devastating direct strike by a typhoon since 03 December 1986. On that date, Super Typhoon Kim passed just to the north of the island causing major damage. The following is an excerpt from an eyewitness account of the effects of Kim on Saipan (Straube, 2005):

> *"Then late on Wednesday, December 3, 1986, super-typhoon Kim lashed into Saipan with torrential rains and winds exceeding 200 m.p.h. … it was comparable to the bombardment … during bombing raids in WW II Frankfurt. … A good part of the local population, however, lived in simple wooden structures, several hundred of which were either blown away that night or washed out to sea. There was no more public water*

supply, and it took the authorities six weeks and longer to re-establish power and water again. All the trees on the island lost their leaves that night. What before was impenetrable rain forest was totally defoliated and suddenly looked like a ghostlike wilderness.

Not to mention the broken-down power lines, flooding sewage, drowned boonie dogs, and the much higher than normal ocean level … Everything was still wet inside. The refrigerator, air conditioning, communications – everything was dead. And it was going to stay so for a while."

This description could well be applied to Typhoon Soudelor for its destructive rampage across the island on the late night of 02 August 2015. In one major aspect, however, Soudelor differed from Kim: the core of Soudelor was so small that it had negligible effects upon the sea, despite well over 100 mph sustained wind.

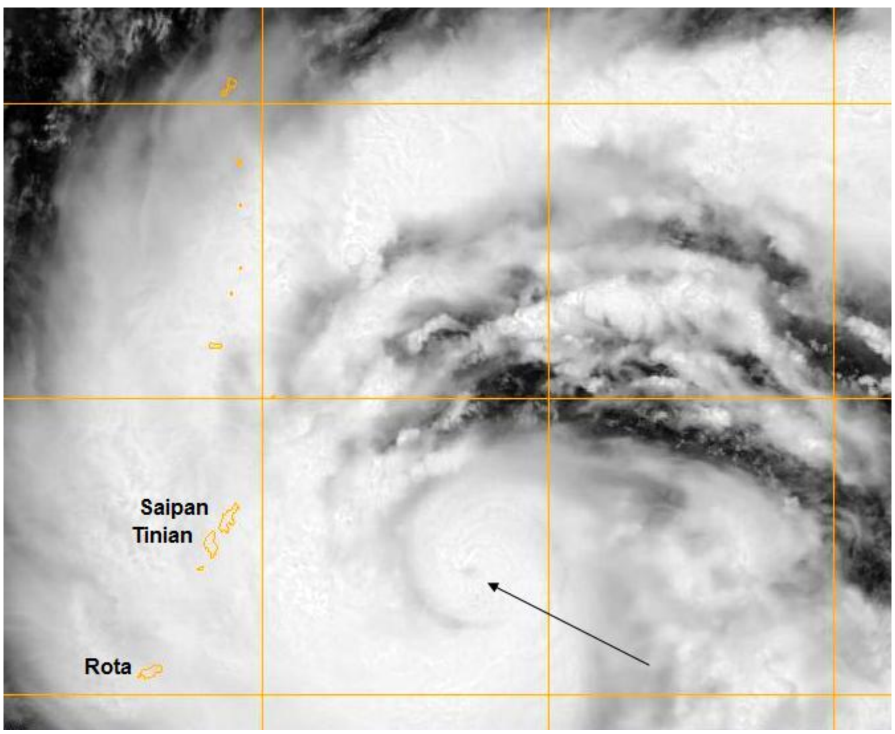

Figure 1. A visible satellite image of Typhoon Soudelor at 1230 PM local time on the afternoon of 02 August 2015. It was, at this time, still at tropical-storm intensity as per the Joint Typhoon Warning Center. The arrow points to the tiny "pinhole" eye in its small core. Extensive outer rain bands nearly encircle the core. Within 12 hours the tiny eye would pass directly over Saipan resulting in severe damage. The north end of Tinian is only 3 miles off the south shore of Saipan, but was largely unharmed by Soudelor! After passing Saipan, the outer rain bands contracted to form a larger secondary eye wall that would surround and destroy the tiny core seen here.

2. Time lines

a. Initial disturbance southwest of Hawaii

During the final week of July, 2015, westerly winds at low latitude had penetrated past the International Date Line all the way east along the equator to the south of Hawaii. This had the effect of replacing the normal trade-wind trough in this region with a monsoon trough. A shift or extension of the western North Pacific monsoon trough well to the east of its normal position is a typical atmospheric response to El Niño. The state of the climate was strong El Niño at the time of the formation of Soudelor. When the 2015 declared El Niño runs its course through early 2016, it is anticipated to rival in intensity and impacts of the epic El Niño events of 1982-83 and 1997-98. The tropical disturbance that became Typhoon Soudelor originated in the central North Pacific in association with the unusual low-latitude westerly winds; but, as Fig. 2 shows, the incipient TC moved west-northwestward away from this zone of low-latitude westerlies to become a more localized cloud cluster overlying a patch of enhanced easterly winds north of the axis of the monsoon trough.

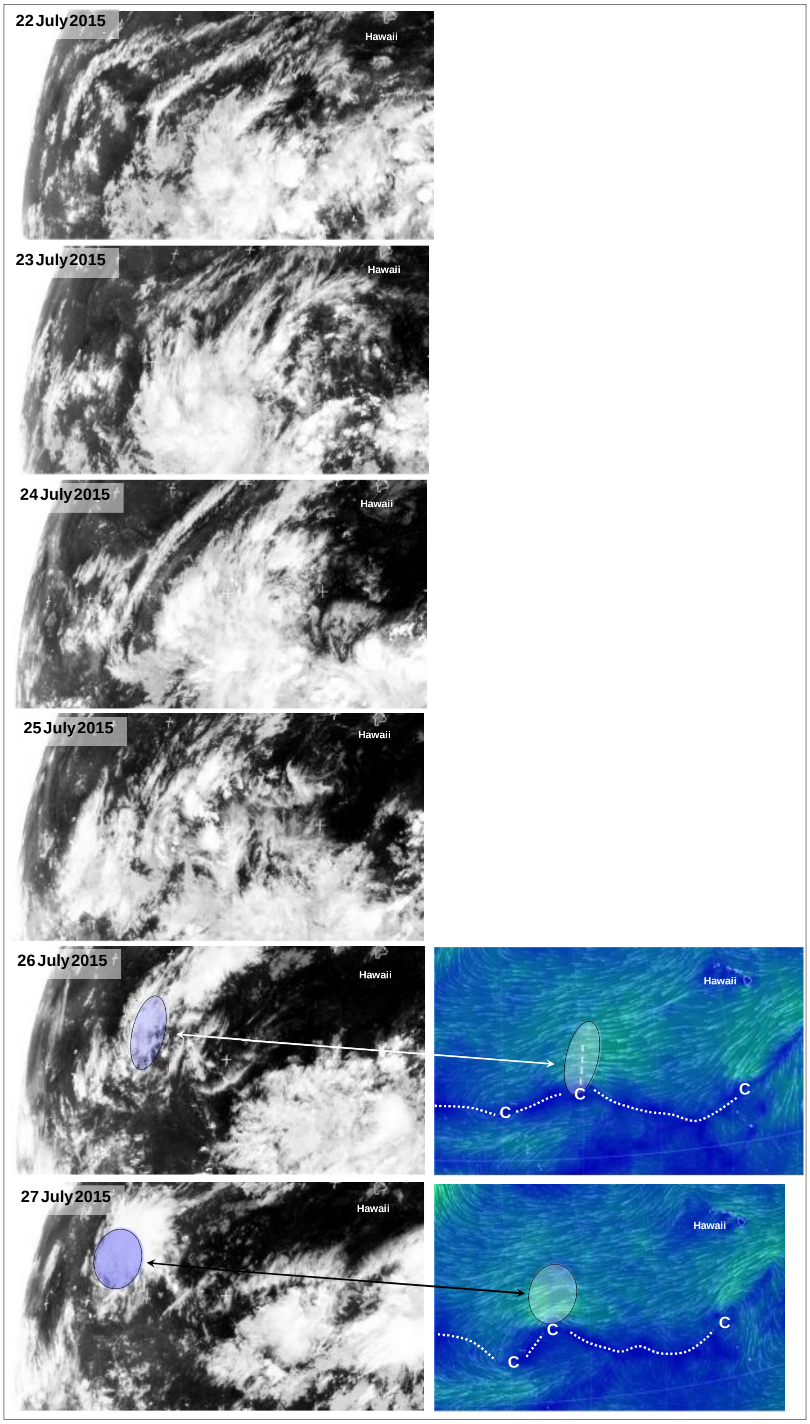

Figure 2. A Hovmoller-type sequence of satellite images showing the formation and westward drift during 22 to 27 July of the tropical disturbance that became Typhoon Soudelor. The surface streamlines (blue and green diagrams in the lower right) show that the discrete cloud cluster that became Soudelor (overlain by semi-transparent ovals) was located in a patch of enhanced easterly wind to the north of the monsoon trough.

Several tropical cyclones prior to Soudelor that affected the islands of Micronesia during the first half of 2015 formed at very low latitude (~ 5° N), and in association with a companion twin tropical cyclone in the Southern Hemisphere. Two cases of named twin tropical cyclones during 2015 incude: Bavi and Pam (March 2015); and, Chan-hom and Raquel (July 2015). One can see from Fig. 3 that one day prior to the JTWC adding the pre-Soudelor disturbance to its list of official INVEST areas, the discrete cloud cluster that would become Soudelor was moving into a region with a pre-existing monsoon trough with in-place enhanced low-latitude westerly winds.

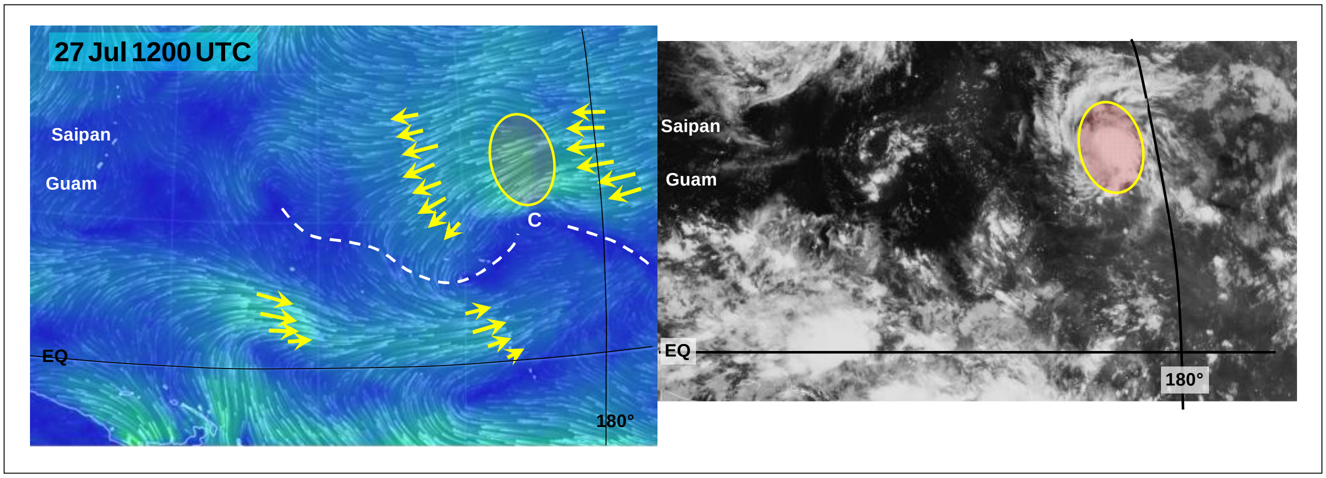

Figure 3. Surface streamlines on the 27th of July showing an in-place monsoon trough (white dashed line) extending across the eastern portion of the western North Pacific. An extended zone of enhanced westerly wind is seen near the equator, with a patch of enhanced easterly low-level flow located underneath the discrete cloud cluster (overlain by transparent ovals on both the streamline chart and the infrared satellite image) that would become Typhoon Soudelor. It is plausible that this monsoon trough interacted with Soudelor to keep its track farther to the south than indicated by the forecast guidance over the next several days.

c. Benchmarks

(1) JTWC

i*. The INVEST AREA*

The JTWC has several procedural milestones and benchmarks that are normally adhered to during the formation and development of a tropical cyclone. The first benchmark is the placement of the area of interest into the status of a numbered INVEST area. These numbers cycle repetitively from 90W through 99W. The “upgrade” of a tropical disturbance to an official numbered INVEST area is more than just a minor meteorological milestone. It awakens the entire academic and institutional support structure (such as the Naval Research Laboratory, Monterey CA and the Cooperative Institute for Meteorological Satellite Studies, Madison WI) who, at the initiation of an INVEST area, begin to offer and post to the world their full suite of tropical cyclone support products such as color-enhanced microwave satellite imagery and automated diagnostic measures of intensity.

***ii**. The Tropical cyclone Formation Alert (TCFA)*

The next milestone in the advisory process used by all U.S. tropical cyclone warning agencies (e.g., the National Hurricane Center, Miami; the Central Pacific Hurricane Center, Honolulu; and, the Joint Typhoon Warning Center, Pearl Harbor) is the Tropical Cyclone Formation Alert (TCFA). A TCFA is issued when a tropical disturbance is anticipated to become a “significant” tropical cyclone within the subsequent 24 hours. A tropical cyclone becomes “significant” when the responsible warning agency issues its first advisory (i.e., Warning Number 1) on a particular tropical cyclone, establishing that cyclone’s number (e.g., TC 13W) and sometimes (if things are happening quickly) the name. As one may surmise, there is some circularity in the meaning of “significant” tropical cyclone, as Warning Number 1 bestows the status of “significant” to a TC. In practice, Warning Number 1 usually begins when a tropical disturbance acquires a distinct and persistent low-level cyclonic vortex with maximum surface wind speeds of 25 or 30 kt. At these wind speeds a tropical cyclone is known as a tropical depression. When wind speeds reach 35 kt or higher, the cyclone becomes a tropical storm and is given a name in addition to its number. The JTWC provided the names of tropical storms in the western North Pacific until the year 2000 when the Japan Meteorological Agency (JMA) became responsible for the naming. The JTWC still provides the official number used throughout Micronesia, but the JMA name is used when any cyclone becomes a tropical storm. It is possible (and has already occurred) that a numbered tropical depression of the JTWC becomes an unnamed tropical storm, or a cyclone is named by the JMA, but remains only a numbered depression as per JTWC.

***iii.** Tropical Depression, Tropical Storm, Typhoon and Super Typhoon*

Tropical cyclones are classified by sustained maximum winds near the surface. The sequence is summarized in Table 1 below.

Table 1. Tropical cyclone designation and associated maximum sustained 1-minute over-water surface wind and peak gust.

Tropical Depression	< 35 kt	G < 45 kt
Tropical Storm	35-60 kt	G 45-70 kt
Typhoon	65-125 kt	G 80-140 kt
Super Typhoon	130 kt or higher	G 150 kt or higher

In practice, sustained winds are given in multiples of 5, with peak gusts (over water) at 122% of the value of the sustained wind. Sustained wind speeds over land are usually lower than they are over open water, but the potential peak gust is the same. Thus, while the sustained wind over land is reduced, the gust ratio increases to 130% to 140%, with 160% being about the upper limit.

(2) Soudelor Benchmarks

i. *INVEST area 93W*

The tropical disturbance that became Typhoon Soudelor was designated by the JTWC as INVEST area 93W at 0600 UTC on the 28th of July, or 24 hours after the images shown in Fig. 2 and Fig. 4. The low-level center was positioned at 13.3° N ; 171.6° E, or about 360 n mi (415 st mi) east-northeast of Kwajalein Atoll. Most of the deep convection associated with this tropical disturbance was located to the north of the low-level center. Kwajalein Atoll experienced some brief heavy rain showers and gusty westerly wind as the disturbance passed to its north. The anticipated track of this disturbance was indicated by numerical guidance to be to the west, with a gradual change of track to the west-northwest taking it somewhere safely north of Saipan in the long term.

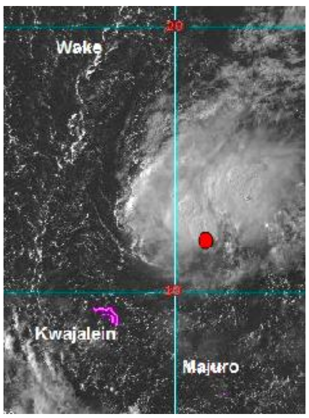

Figure 4. Visible Satellite image of the tropical disturbance that would become Typhoon Soudelor. At this time (4 PM local time, 28 July 2015), the low-level center of the disturbance is located about 360 n mi to the northeast of Kwajalein Atoll. It is at this time that the JTWC added this system to its suite of advisory products as INVEST area 93W.

ii. *Tropical cyclone Formation Alert (TCFA)*

At 14:30 UTC on July 29, the JTWC issued a Tropical Cyclone Formation Alert for the system that would become Typhoon Soudelor. Moving steadily westward, the system was located 365 n mi northwest of Kwajalein and 405 n mi northeast of Pohnpei Island when the TCFA was issued by the JTWC (Fig. 5).

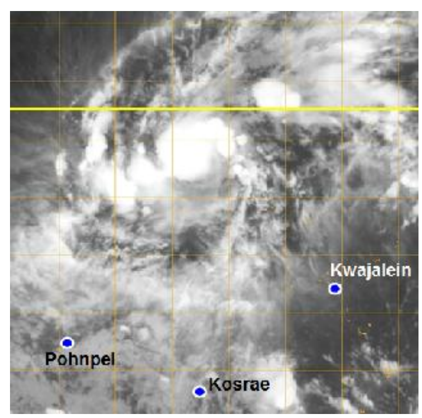

Figure 5. Infrared satellite image of pre-Soudelor at the time of the JTWC formation alert for it. Yellow line shows the latitude of Saipan.

iii. Upgrade to Tropical Depression

In the late afternoon of 30 July, the JTWC issued Warning Number 1 for Tropical Depression 13W. The cyclone had moved so that it was now located approximately 390 n mi to the north-northeast of Pohnpei Island (Fig. 6).

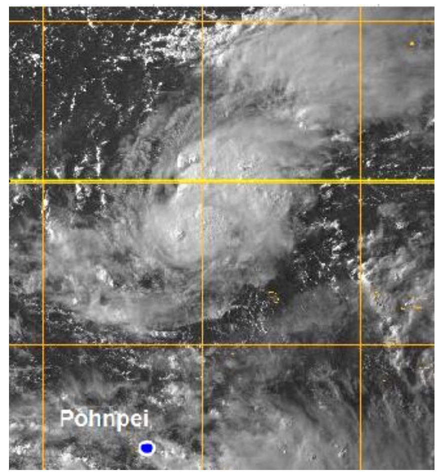

Figure 6. Visible satellite image of TD 13W at the time of JTWC's warning number 1. Yellow line shows the latitude of Saipan.

iv. Upgrade to Tropical Storm

Six hours after issuing the first advisory on Tropical Depression 13W, the JTWC upgraded it to a tropical storm on Warning Number 2 (Fig. 7). JMA also named it Soudelor at this time. The name Soudelor is an entry in the JMA name list provided by the Federated States of Micronesia. It is a Pohnpeian word for a legendary chief. There is no special significance for JMA's choice of this name – it was just the next name on the list.

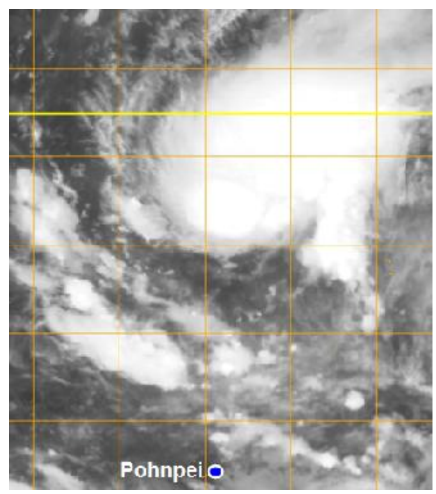

Figure 7. Infrared satellite image at the time of JTWC's upgrade of the system to tropical storm intensity. The JMA was synchronized with the JTWC, and named it Soudelor at this time. Yellow line shows the latitude of Saipan.

v. Upgrade to Typhoon

vi. Upgrade to Super Typhoon

d. Working Best Track Summary

(1) Position

Soudelor had a long straight-moving track that spanned the length of the entire western North Pacific from the International Date Line to the east coast of China (Fig. 8). Impacts were severe on Saipan, Taiwan and mainland China.

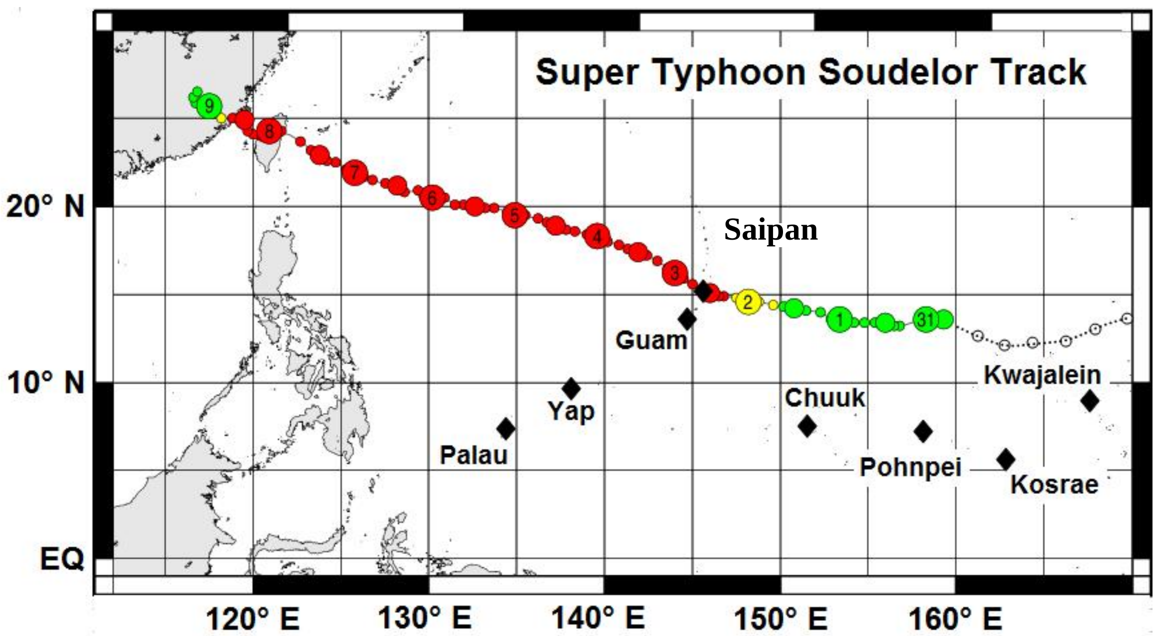

Figure 8. This best track summary was adapted from an on-line utility of the Japan Meteorological Agency. Green indicates tropical storm intensity, yellow indicates severe tropical storm intensity (i.e., maximum sustained winds of Beaufort “storm” category = 47.6 to 63.4 kt) and red indicates typhoon intensity.

(2) Intensity

The real-time JTWC warning intensity estimates of Soudelor increase slowly until just prior to its landfall in Saipan (Fig. 9). After passing Saipan, Soudelor reached a peak intensity of 155 kt sustained 1-minute wind. This elevated Soudelor to the most intense tropical cyclone in the Northern Hemisphere for all of 2015 to-date.

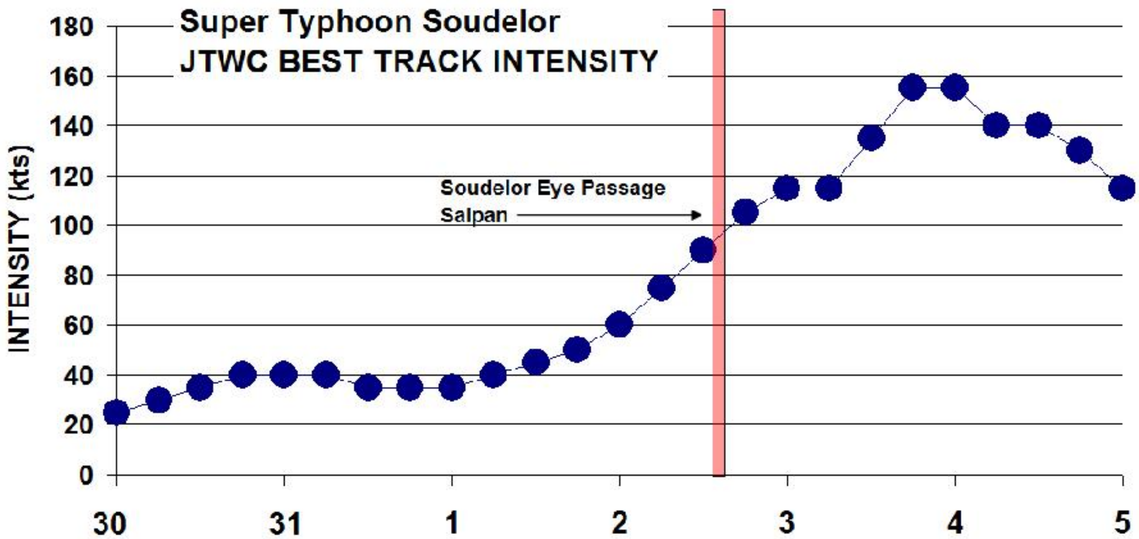

Figure 9. Data for the creation of this best track summary of Soudelor's intensity (as per the JTWC) was obtained from the CIRA RAMMB web site. Values shown are warning intensities at 6-hour intervals from 0000 UTC July 30, 2015 through 0000 UTC o5 August 2015. The partially transparent red bar shows the timing of eye passage over Saipan that occurred during a one-hour window from 1330 UTC to 1430 UTC 02 August 2015 (locally from 1130 PM 02 August to 1230 AM 03 August). The eye passage occurs as the best track intensity is rising from 90 kt at 1200 UTC 02 August to 105 kt at 1800 UTC 02 August.

Later in this report is found the Saipan MET assessment team best-track, which is different from the JTWC best-track; particularly at the time of eye passage over Saipan.

3. The Unique Structure of Soudelor

Super Typhoon Soudelor had unusual structural characteristics and structural evolution during its trek across the western North Pacific. The most unusual structural characteristics occurred during the time of Soudelor's passage over Saipan. At that time, the typhoon possessed a "midget"-sized core with a pinhole eye (Fig. 1 and Fig. 10). A day or so after passing over Saipan, Soudelor underwent a complete eyewall replacement cycle that saw the midget core of its Saipan passage completely surrounded and then destroyed by a contracting secondary eyewall.

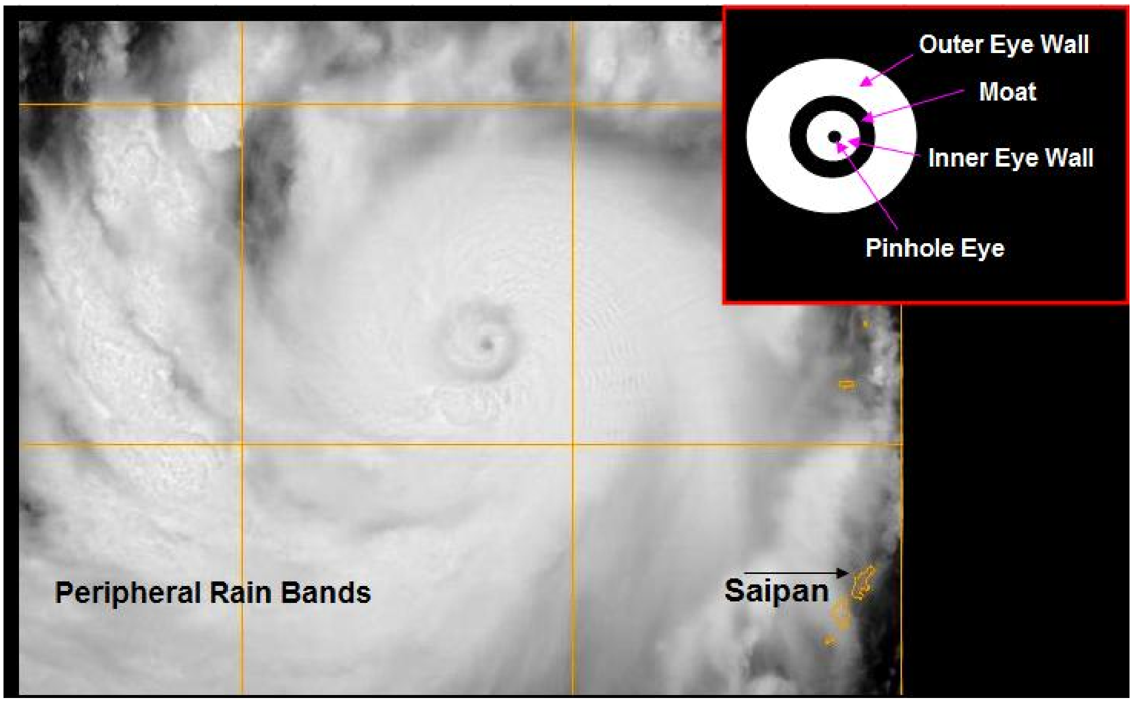

Figure 10. The structure of Soudelor a day after its passage over Saipan. In this visible image the midget core (small inner eye wall surrounding a pinhole eye) is still intact. The midget core will not survive much longer, as the outer eye wall has already completely surrounded it and will soon destroy it, leaving behind only one larger eye with its thick outer eye wall. The inset is a cartoon illustrating the components of Soudelor's structure at the time of the visible satellite image.

Before further discussing Soudelor's structure, it will be helpful to explore some of the terms used; for example: "midget" core, pinhole eye and secondary eye wall formation.

Part 1. Useful Concepts for Analyzing Soudelor

1. Terminology

a. Midget Tropical Cyclones

The *Mame-Taifu* (literally translated from Japanese as "bean typhoon" and figuratively as "midget typhoon") was recognized for many years in Japan as a distinct variety of tropical cyclone. During the first few decades following the inception in the late 1800s of the governmental weather service in Japan, several midget typhoons struck Japan with a landfall intensity which surprised forecasters and severely impacted an unprepared populace (Arakawa 1952). Arakawa writes:

"Small storms of typhoon intensity have been greatly underestimated in the occidental literature. In fact, it is hard to find any mention of them in standard texts in English, German, or French. But in Japan, very small storms of this type often caused great damage during the three fourth century since the inauguration of [the] *Japanese Weather Service. Very small storms of typhoon intensity, mame-taifu in Japanese, are so small that they caused great damage before storm warnings have been issued by the Governmental weather service."*

In 1945, the U.S. Navy implemented several tropical-cyclone tracking centers in the western North Pacific. Routine penetration by Navy reconnaissance aircraft into typhoons began in 1945 and by the Air Force in 1947. On May 01, 1959, the Commander in Chief, Pacific Command, combined Air Force and Navy tracking centers into a command jointly manned by the Navy and Air Force: the Joint Typhoon Warning Center (JWTC), located on Nimitz Hill, Guam. Accounts of peculiar very small typhoons began to accumulate in the Annual Typhoon Reports issued by the Navy's Typhoon Tracking Center (Fleet Weather Central, 1948-1958) and in the Annual Typhoon Report (renamed the Annual Tropical Cyclone Report (ATCR) in 1980) issued by the JTWC (JTWC, 1959- present). Another early acknowledgement by a western scientist of the existence of midget tropical cyclones in the western North Pacific occurred during the years of atomic testing by the United States in the Marshall Islands when a member of the meteorology team assigned to the project, Dr. C.E. Palmer, wrote a personal letter to Arakawa concerning the occurrence of very small storms of typhoon intensity in that region (Arakawa, 1952).

A few unusually small tropical cyclones have also been observed in the Atlantic. In September 1966, a reconnaissance flight through Hurricane Inez reported a minimum seal level pressure of 927 hPa and a maximum flight level wind of 175 knots; yet, it was incredibly compact with a 12 n mi eye, and with hurricane-force winds extending outward from the center only 21 n mi to the southwest and 29 n mi to the northeast (Hawkins and Rubsam, 1967). Hawkins and Rubsam proposed that such storms be called "micro-hurricanes."

Brand (1972) examined the climatology of very large and very small typhoons in the western North Pacific. He classified a typhoon as "very small" if the mean radius to the outer closed isobar was less than 2° (222 km) of great–circle arc. Brand recognized both historical terms for very small tropical cyclones — Arakawa's "midget typhoons" and Hawkin's and Rubsam's "micro-hurricanes"— but, by the early 1970s, the term "midget" had gained ascendancy in popular usage in the forecasting community as a descriptor for tropical cyclones of unusually small size.

(2) Pinhole eye

The problems with intensity forecasts include large errors in cases involving rapid intensity change. In recent years several tropical cyclones that underwent rapid intensification developed a very small eye in the process, often referred to as a 'pinhole' eye. The term pinhole eye is a colloquial term that is now well dispersed across the tropical cyclone community and has made its way into several papers in the gray literature (e.g., Musgrave et al. 2008, Mooney 2006, and Gutro 2015). The term achieved lasting fame when it was used in the official National Hurricane Center discussion on Hurricane Wilma (2005), which had one of the most spectacular "pinhole" eyes of all:

> HURRICANE WILMA DISCUSSION NUMBER 14
> NWS TPC/NATIONAL HURRICANE CENTER MIAMI FL
> 11 PM EDT TUE OCT 18 2005
>
> WILMA HAS DEVELOPED **THE DREADED PINHOLE EYE**. REPORTS FROM THE AIR FORCE RESERVE HURRICANE HUNTER INVESTIGATING WILMA BETWEEN 19Z AND 23Z INDICATED A 7-8 N MI WIDE EYE...WITH THE CENTRAL PRESSURE DROPPING FROM 970 MB TO 954 MB IN 3 HR 14 MIN. THE MAXIMUM FLIGHT-LEVEL WINDS MEASURED BY THE AIRCRAFT AT 850 MB WERE 101 KT. SINCE THAT TIME... SATELLITE IMAGERY SHOWS INCREASED ORGANIZATION...WITH A RING OF COLD TOPS OF -80C TO -87C SURROUNDING THE EYE. SATELLITE INTENSITY ESTIMATES ARE 102 KT FROM TAFB AND SAB...AND 90 KT FROM AFWA. BASED ON THIS AND EXTRAPOLATION OF THE LAST AIRCRAFT DATA...THE INITIAL INTENSITY IS INCREASED TO 95 KT. THIS MAY BE CONSERVATIVE.

In the Musgrave et al. paper, pinhole eyes are defined as those eyes with a diameter smaller than 10 n mi, representing less than ten percent of the eye size measurements available in aircraft reconnaissance fixes. While pinhole eyes made up less than 10% of the total sample of eye diameter estimates, those estimates were spread out amongst 38 of the 99 TCs represented in their sample of aircraft reconnaissance data. The following finding is useful for an evaluation of Soudelor over Saipan:

> *"Half of the tropical cyclones that reached major hurricane intensity on the Saffir-Simpson scale had at a pinhole eye for at least one eye diameter estimate. Of the TCs with a pinhole eye, approximately 60% reached major hurricane intensity."*

The eye of Soudelor when over Saipan certainly can unashamedly take its place in the pinhole eye hall of fame!

(3) Secondary eye wall formation and the eye wall replacement cycle

In order to summarize this topic in a short space, the Wikipedia entry for this topic is satisfactory:

Eyewall replacement cycles, also called concentric eyewall cycles, naturally occur in intense tropical cyclones, generally with winds greater than 115 mph (100 kt), or major hurricanes (Category 3 or above). When tropical cyclones reach this intensity, and the eyewall contracts or is already sufficiently small, some of the outer rainbands may strengthen and organize into a ring of thunderstorms—an outer eyewall—that slowly moves inward and robs the inner eyewall of its needed moisture and angular momentum. Since the strongest winds are in a cyclone's eyewall, the tropical cyclone usually weakens during this phase, as the inner wall is "choked" by the outer wall. Eventually the outer eyewall replaces the inner one completely, and the storm may re-intensify.

The discovery of this process was partially responsible for the end of the U.S. government's hurricane modification experiment Project Stormfury. This project set out to seed clouds outside the eyewall, apparently causing a new eyewall to form and weakening the storm. When it was discovered that this was a natural process due to hurricane dynamics, the project was quickly abandoned.

Almost every intense hurricane undergoes at least one of these cycles during its existence. Recent studies have shown that nearly half of all tropical cyclones, and nearly all cyclones with sustained winds over 127 mph (110 kt) undergo [one or more] eyewall replacement cycles.

Soudelor underwent a dramatic eyewall replacement after it passed over Saipan. The pinhole eye it possessed when it passed over Saipan was nearly and order of magnitude smaller than the eye it had after the replacement was complete (Fig. 11).

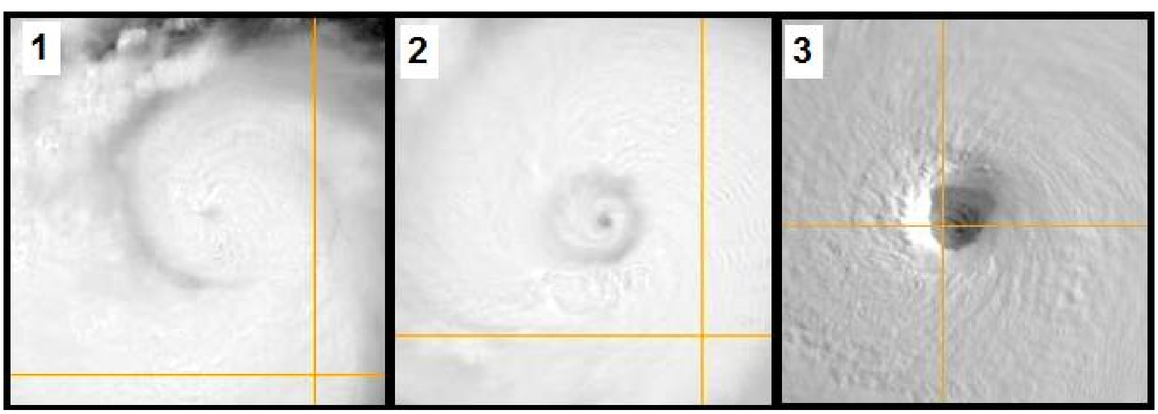

Figure 11. The eyewall replacement cycle of Soudelor: (1) the pinhole eye prior to Saipan landfall; (2) a concentric eyewall structure a day after Saipan landfall; and (3) the much larger eye that resulted at the end of the cycle. Picture times are: (1) 12:30 PM 02 August; (2) 1 PM 03 August; and, (3) 7:30 AM 04 August. Images are at same scale (2 x 2 degrees).

(4) Tropical cyclone spawned tornadoes

It was a common perception of Saipan residents that the eyewall of Soudelor was accompanied by tornadoes during its crossing of the island. Intense wind gusts, scattered pockets of heavy damage, and trees close to one another fallen in opposite directions contributed to this perception. (For the finding of the Soudelor MET assessment team regarding the possible occurrence of tornadoes, see Part 2.)

Tornadoes make a significant contribution to the dangers and impacts associated with landfalling hurricanes in the United States. Nearly every tropical cyclone of full hurricane intensity whose center crosses the U.S. Gulf of Mexico or Atlantic coastline has associated tornadoes, while over half (60%) of landfalling tropical storms spawn tornadoes (Gentry, 1983). Tornadoes contribute up to 10% of the overall fatalities and up to a half percent of the overall damage caused by the hurricanes that spawn them (Novlan and Gray, 1974). Most hurricane-spawned tornadoes are relatively weak, but there are many exceptions. A tornado associated with Hurricane Allen (1980) caused $50 million in damage to the city of Austin Texas. This tornado was ranked F2 on the Fujita Scale. Another tornado near San Marcos, Texas, on the same day, reached F3. Some hurricanes spawn many tornadoes. The record-holder is Hurricane Beulah (1967). One hundred fifteen tornadoes are known to have occurred in association with Hurricane Beulah (Orton, 1970). Excluding Beulah, the average hurricane which spawned tornadoes had ten (Novlan and Gray, 1974).

Hurricane-spawned tornadoes are most frequent at the time when their parent hurricane initially crosses land and is undergoing rapid filling (Novlan and Gray, 1974). Most form in association with the outer rainbands of the hurricane, while about 20% are found with the inner bands or near the outer edge of the eyewall (Gentry, 1983). Smith (1965) proposed a model that established the right front quadrant (with respect to storm motion) as the “significant tornado sector”. Orton (1970) showed that a frame of reference to true north versus the directional heading of the hurricane yielded the narrowest clustering of tornadoes. The preferred sector for tornadoes in a true-north reference frame extends from 350° to 120° azimuth and 60 - 250 n mi out from the storm center (Fig. 12).

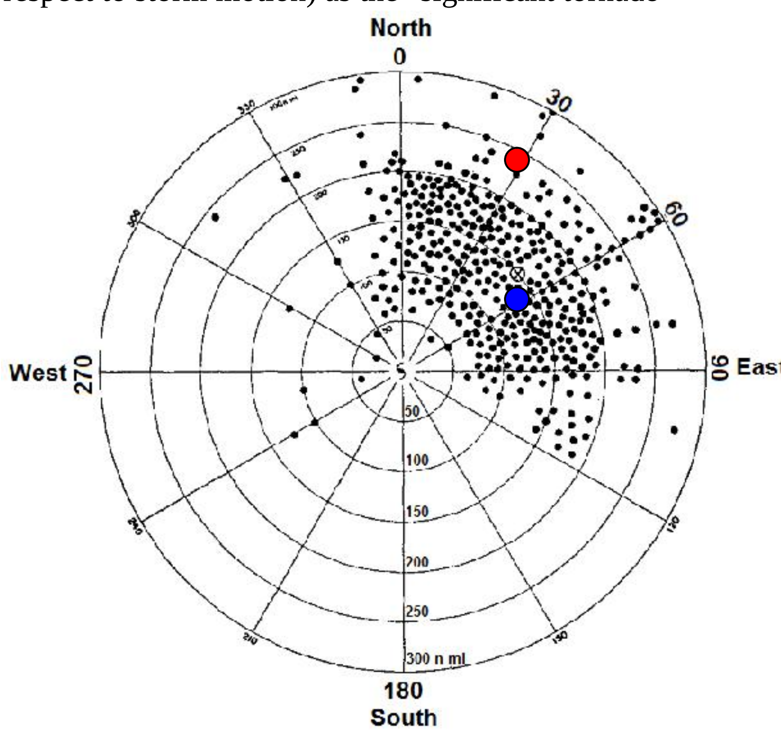

Figure 12. A plan view display of 373 U.S. hurricane tornadoes (1948-72) with respect to the hurricane center. The blue dot refers to the centroid of all cases. The red dot is the centroid of 68 Japanese typhoon-spawned tornadoes.

(5) Sustained wind and gusts

There are many types of anemometers (e.g., Fig. 13) designed to measure wind speeds including: cup; vane; hot wire; laser Doppler; Sonic; ping-pong ball; plate; and tube. When Dr. John Thomas Romney Robinson, of Armagh (Ireland) Observatory first designed his four-cup anemometer, he asserted that the cups moved one-third of the speed of the wind, unaffected by the cup size or arm length. This was apparently confirmed by some early independent experiments, but it was incorrect. Instead, the ratio of the speed of the wind and that of the cups, the anemometer factor, depends on the dimensions of the cups and arms, and may have a value between two and a little over three. Every previous experiment involving an anemometer had to be repeated.

The three-cup anemometer developed by the Canadian John Patterson in 1926 and subsequent cup improvements by Brevoort & Joiner of the USA in 1935 led to a cupwheel design which was linear and had an error of less than 3% up to 60 mph (97 km/h). Patterson found that each cup produced maximum torque when it was at 45 degrees to the wind flow. The three-cup anemometer also had a more constant torque and responded more quickly to gusts than the four cup anemometer.

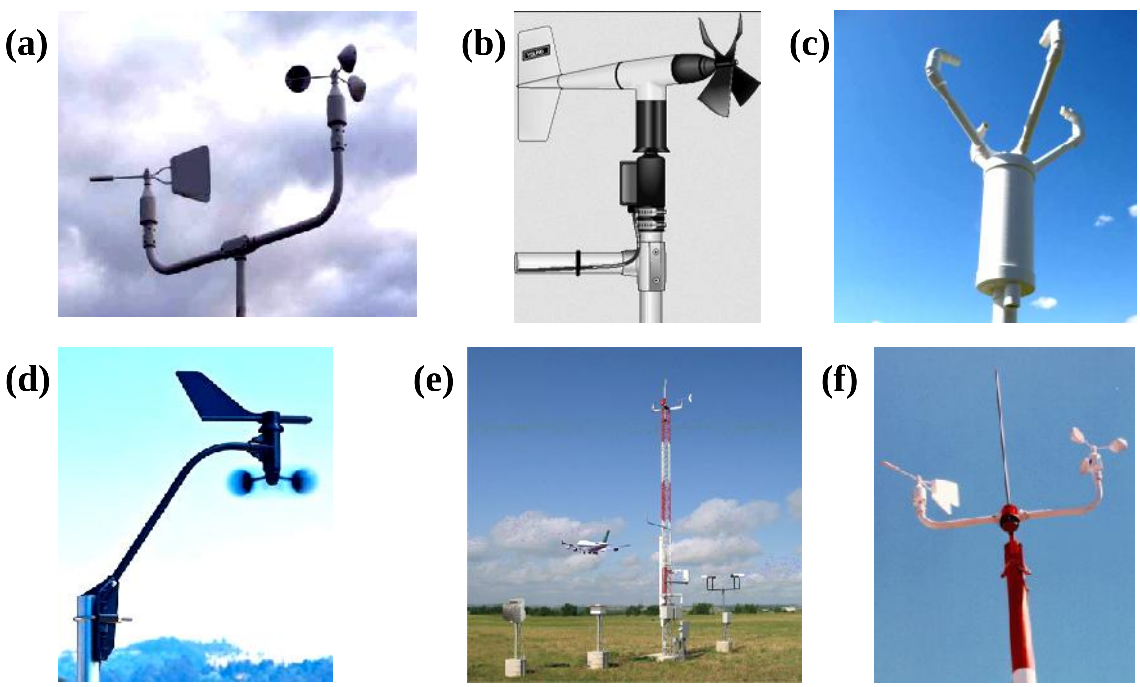

Figure 13. Some commonly used anemometers: (a) three-cup with adjacent directional vane; (b) vane type with propeller; (c) ultrasonic; (d) three-cup and wind vane of the Davis Pro© home weather station; (e) an ASOS tower with a three cup anemometer and adjacent directional vane; and (f) close-up of the ASOS wind sensors.

The highly successful metal pressure tube anemometer of William Henry Dines in 1892 (Fig. 14) utilized the pressure difference between the open mouth of a straight tube facing the wind and a ring of small holes in a vertical tube which is closed at the upper end. Both are mounted at the same height. The pressure differences on which the action depends are very small, and special means are required to register them. The recorder consists of a float in a sealed chamber partially filled with water. The pipe from the straight tube is connected to the top of the sealed chamber and the pipe from the small tubes is directed into the bottom inside the float. Since the pressure difference determines the vertical position of the float this is a measured of the wind speed.

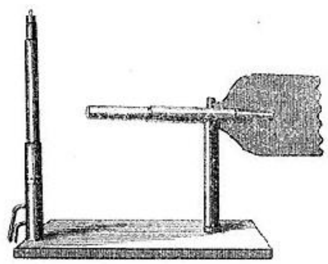

Figure 14. Tube anemometer invented by William Henry Dines. The movable part (right) to be put on top of the fixed part (left).

The Dines anemometer was a mainstay of wind speed measurements for most of the 20th Century and forms a substantial portion of the historical wind records. Three-cup anemometers are currently used as the industry standard for wind resource assessment studies. The U.S. National Weather Service Automated Surface Observing System (ASOS) uses a three-cup anemometer to measure wind speed (Figs. 13e and 13f). Propeller instruments and ultrasonic anemometers are also widely used. Hot wire anemometers used at U.S. Air Force bases in the 1990s were deemed unsuitable for tropical cyclone observation. One such anemometer was responsible for the discredited world record peak-gust candidate of 236 mph recorded at Andersen Air Force Base, Guam, during Typhoon Paka (1997).

Two important wind metrics include the “sustained” wind and the “gust”. Most weather agencies use the definition for sustained winds recommended by the World Meteorological Organization (WMO), which specifies measuring winds at a height of 10 m (33 ft) for 10 minutes, and then taking the average. However, the United States National Weather Service defines sustained by averaging winds over a period of one minute, measured at the same 10 m (33 ft) height. In operational practice the sustained one-minute wind, say at 8 PM, is the highest one-minute wind that occurs within the 10 minute interval prior to the valid time of the observation (i.e., 7:50 PM to 8 PM). Done in this fashion, the value of the highest one-minute sustained wind is approximately 14% greater than the ten-minute sustained wind over the same period. The gust is the highest “instantaneous” wind measured over any selected time interval. It never is truly instantaneous since there are inherent lags in the ability of the instrumentation to respond. For cup anemometers with pen recording charts, it is considered to be 2 seconds (Krayer and Marshall, 1992). Holmes and Ginger (2012) showed that the equivalent moving averaging time for the damped resonant response of the Dines anemometers in relation to the maximum gusts produced is equivalent to about 0.2 s. They also produced factors to convert gust wind speeds using a 3-cup anemometer and 3s averaging to a gust with an equivalent averaging time of 0.2 s. In the United States, ASCE 7 (2010) changed to a peak gust wind speed metric from the previous ‘fastest mile’ definition in 1995, and similar gust speeds have continued since then. The analysis for non-hurricane regions used gusts recorded primarily from cup anemometers with a corresponding 'time constant' (roughly equivalent to the gust duration) of about 0.5 s. However, design peak gust speeds in the hurricane-affected regions of the US have been generated by simulation methods, with gust factors equivalent to 3 s moving average gusts, similar to the WMO definition. Thus, the wind speed used in design for tropical cyclone resiliency is often referred to as a "3-second gust". This description of a gust as a "3-second gust" is misleading, as it was based on an earlier definition of the averaging time of the gust recorded by the Dines anemometers, and is not a moving-average (Ginger, 2011). A thorough theoretical treatment of gust wind speeds for design of structures (Ginger, et al., 2013) is reproduced in Appendix X.

Another important factor to consider is the ratio of the gust to the sustained wind, or the "gust factor". A gust factor is a theoretical conversion between an estimate of the mean wind speed and the expected highest or "gust" wind speed of a given duration within a stated observation period. This concept is applicable only in a statistical sense, and isolated comparisons cannot be expected to match theoretical values. Gust factors vary substantially depending on exposure. To be representative, certain conditions must be met, many of which may not be exactly satisfied during a specific weather event or at a specific location.

The US National Hurricane Center, the Central Pacific Hurricane Center and the JTWC imply a one minute averaging time for their reported sustained winds in tropical cyclones. Since the inauguration of the Automatic Surface Observation System (ASOS) the National Weather Service has adopted a two minute average standard for its sustained wind definition. This is because the ASOS stations average and report their wind data over a two minute period. There is no conversion factor used to change a two minute average wind into a one minute average wind, and it is pointless to try to estimate the highest one minute wind over a two minute period, as they are essentially the same. The sustained wind speeds and associated gusts in tropical cyclones has for a long time been standardized to the over-water one-minute sustained wind with an associated peak gust that is approximately 123% of the one-minute wind (see Table 2).

1-MIN Sustained	**(kt) Gust**
30	40
35	45
40	50
45	55
50	60
55	65
60	70
65	80
70	85
75	90
80	100
85	105
90	110
95	115
100	120
105	130
110	135
115	140
120	145
125	150
130	160
135	165
140	170
145	175
150	185
155	190
160	195
165	200
170	210

Exposure at +10 m		Reference Period	Gust Factor G_{τ,T_o}				
			Gust Duration τ (s)				
Class	Description	T_o (s)	*3*	*60*	*120*	*180*	*600*
In-Land	Roughly open terrain	3600	1.75	1.28	1.19	1.15	1.08
		600	1.66	1.21	1.12	1.09	1.00
		180	1.58	1.15	1.07	1.00	
		120	1.55	1.13	1.00		
		60	1.49	1.00			
Off-Land	Offshore winds at a coastline	3600	1.60	1.22	1.15	1.12	1.06
		600	1.52	1.16	1.09	1.06	1.00
		180	1.44	1.10	1.04	1.00	
		120	1.42	1.08	1.00		
		60	1.36	1.00			
Off-Sea	Onshore winds at a coastline	3600	1.45	1.17	1.11	1.09	1.05
		600	1.38	1.11	1.05	1.03	1.00
		180	1.31	1.05	1.00	1.00	
		120	1.28	1.03	1.00		
		60	1.23	1.00			
At-Sea	> 20 km offshore	3600	1.30	1.11	1.07	1.06	1.03
		600	1.23	1.05	1.02	1.00	1.00
		180	1.17	1.00	1.00	1.00	
		120	1.15	1.00	1.00		
		60	1.11	1.00			

(6) Horizontal structure of the typhoon wind field

There are two broad classes of atmospheric cyclonic storm systems: (1) Tropical cyclones; and, (2) Extratropical (or, mid-latitude) cyclones. We will leave aside, for now, other specialized or parochial cyclone types such as the sub-tropical cyclone, polar lows and monsoon depressions. Because much of the legend and lore of tropical meteorology was developed in the Atlantic, we have the following (rather parochial) list of characteristics of a tropical cyclone:

One complication with the use of the 1 min averaging time for the standard for sustained wind in the Atlantic and Northeast Pacific tropical cyclone basins (where the United States has the official World Meteorological Organization tropical cyclone advisory responsibilities) is that in most of the rest of the world, a 10 min averaging time is utilized for "sustained wind". While one can utilize a simple ratio to convert from peak 10 min wind to peak 1 min wind (roughly 12% higher for the latter), such systematic differences to make interbasin comparison of tropical cyclones around the world problematic.
The maximum sustained wind mentioned in the advisories that NHC issues for tropical storms and hurricanes are the highest 1 min surface winds occurring within the circulation of the system. These "surface" winds are those observed (or, more often, estimated) to occur at the standard meteorological height of 10 m (33 ft) in an unobstructed exposure (i.e., not blocked by buildings or trees)
.

The previous versions of the Standard
Incorrectly referred
to ‘a gust of 2 to 3 seconds duration’ as the
basic
wind speed, which originated from
the report
by Whittingham (1964).

„
Extreme Windspeed Baseline Climate Investigation Project: Summary Page 6 of
31
misleading, as it was based on an earlier definition of the averaging time of the gust recorded by the Dines anemometers, and is not a moving-average

In the United States, the wind speed used in design is often referred to as a "3-second gust" which is the highest sustained gust over a 3-second period having a probability of being exceeded per year of 1 in 50 (ASCE 7-05). This design wind speed is accepted by most building codes in the United States and often governs the lateral design of buildings and structures.

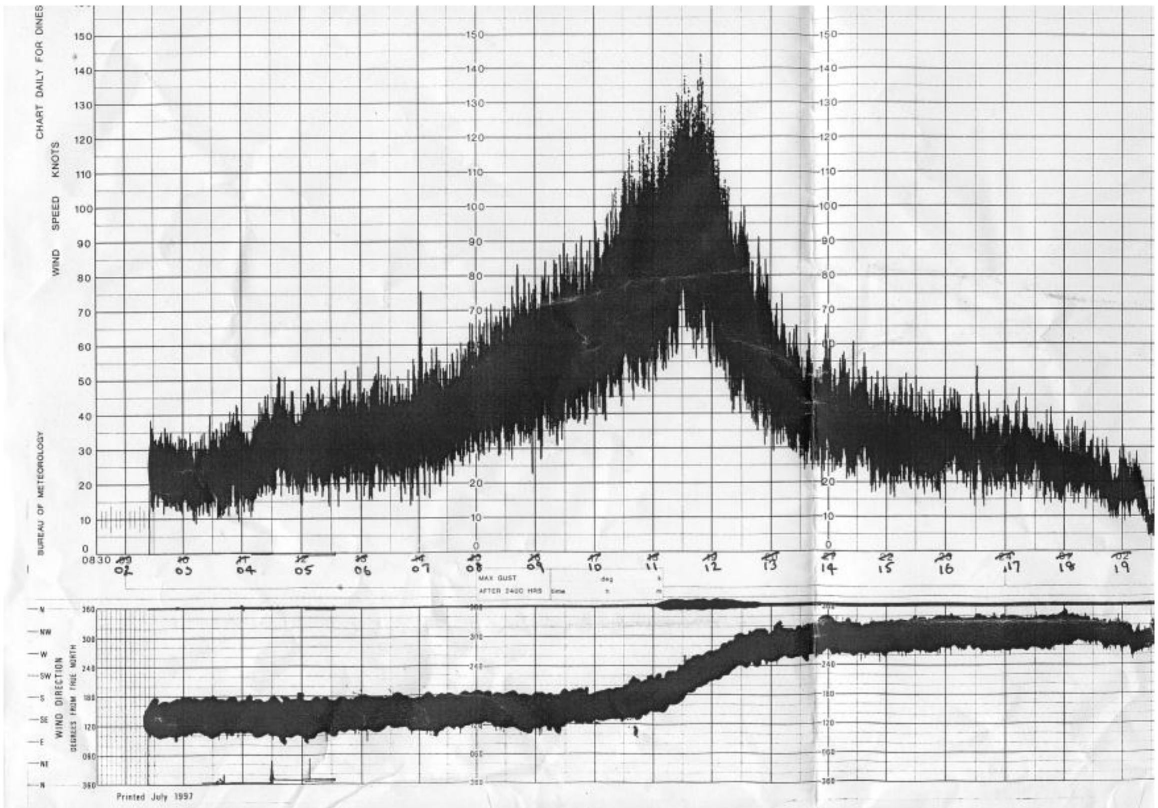
CHART DAILY FOR DINES
WIND SPEED KNOTS
BUREAU OF METEOROLOGY
MAX GUST
AFTER 2400 HRS
WIND DIRECTION
DEGREES FROM TRUE NORTH
Printed July 1997

pinhole eyes are defined as those eyes with a diameter smaller than 10 n mi, representing less than ten percent of the eye size measurements available in aircraft reconnaissance fixes. A combination of aircraft reconnaissance fixes, operationally-estimated size parameters, and synoptic data is used to examine the size and intensification properties of pinhole cases, as well as their large-scale environment.

28th Conference on Hurricanes and Tropical Meteorology

17C.7

Pinhole eyes in tropical cyclones

Kate D. Musgrave, Colorado State University, Fort Collins, CO; and W. H. Schubert and C. A. Davis

Session 17C, Tropical Cyclone Structure V: Eye and Eyewall Structure
Friday, 2 May 2008, 8:00 AM-9:45 AM, Palms H

PINHOLE EYES IN TROPICAL CYCLONES

Musgrave, Kate D., W. H. Schubert, and C. A. Davis. "17C. 7 PINHOLE EYES IN TROPICAL CYCLONES."
17C.7 Pinhole eyes in tropical cyclones (2008 **...**
May 2, 2008 **...** 17C.7. Pinhole eyes in tropical cyclones. **Kate D**. **Musgrave**, Colorado State University, Fort Collins, CO; and **W. H. Schubert and C. A. Davis**.
https://ams.confex.com/ams/28Hurricanes/.../paper_138273.htm

Kate D. Musgrave
1
, W. H. Schubert
Discover magazine The Dreaded Pinhole Eye By Chris Mooney | August 29, 2006 6:56 pm

The Dreaded Pinhole Eye
By Chris Mooney | August 29, 2006 6:56 pm

\ and C. A. Davis
Colorado State University, Fort Collins, CO
National Center for Atmospheric Research, Boulder, CO

Satellite sees Hurricane Blanca develop a pinhole eye June 3, 2015 by Rob Gutro
http://phys.org/news/2015-06-satellite-hurricane-blanca-pinhole-eye.html

(7) The Dvorak Techniques

The first weather satellite, Vanguard 2, was launched on February 17, 1959. It was designed to measure cloud cover and resistance, but a poor axis of rotation and its elliptical orbit kept it from collecting a notable amount of useful data. The Explorer VI and VII satellites also contained weather-related experiments. The first weather satellite to be considered a success was TIROS-1, launched by NASA on April 1, 1960. TIROS operated for 78 days and proved to be much more successful than Vanguard 2. The launch of TIROS I (Television and InfraRed Observation Satellite) on April 1, 1960 marked the first day it became possible to observe the Earth's weather conditions on a regular basis, over most of the world from the vantage point of outer space. When the satellite data was read out at either of the ground stations, it was recorded on 35-mm film for making prints and large projections. From these, a hand-drawn cloud analysis (nephanalysis) was made then transmitted by facsimile to the U.S. Weather Bureau National Meteorological Center (NMC) near Washington, D.C. It was not until 1962 (TIROS IV, TIROS V) that some of the actual gridded satellite pictures were sent via facsimile to NMC and some other large Weather Bureau offices.

TIROS 1 was rocketed into space aboard a Thor-Able launch vehicle, in the early hours of April 1, 1960, from Cape Canaveral, Florida.

First picture obtained from the TIROS 1 weather satellite shows a cloud band stretching across New England and out to sea south of Nova Scotia.

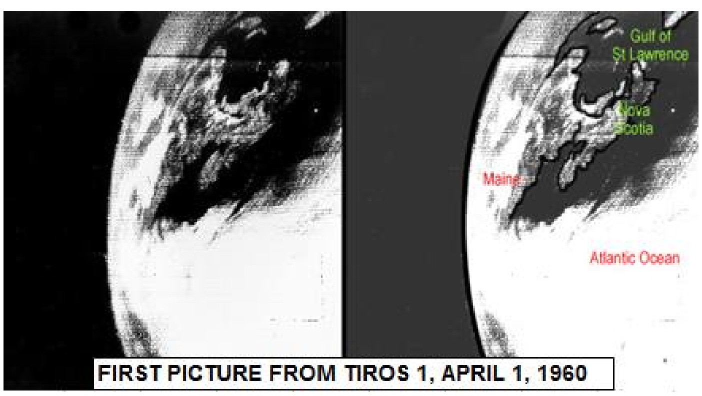

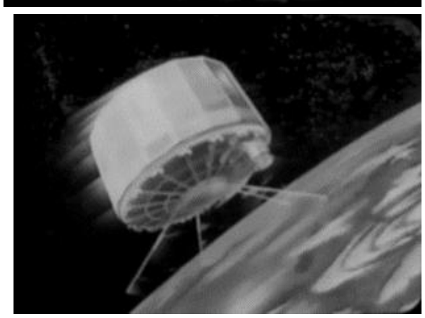

Television promotional advert for TIROS program.

Hurricane Esther was the first large tropical cyclone to be discovered by satellite imagery, though not the first to be imaged by one. On September 10, 1961, TIROS III observed an area of convection, or thunderstorms, to the southwest of the Cape Verde islands, suggesting the possibility of tropical cyclogenesis. S. Fred Singer, Deputy Assistant Secretary for Scientific Programs, Department of the interior, provided this account of the photo-capture of Esther:

"Esther was the first hurricane to be discovered by a satellite, but Tiros III also took valuable pictures of Anna, Betsy, Carla, and Debbie in 1961. In all cases, the Tiros pictures provided important supplements to reconnaissance aircraft observations and to data obtained by ground-based observations, by fixing the position of the hurricane center and showing the extent of the spiral cloud bands. …

"Esther will be assured a place in meteorological history. She was the first hurricane to be discovered by satellite, moved in a complex loop off the east coast of the United States, threatening New England, and was the guinea pig for a seeding experiment with silver iodide."

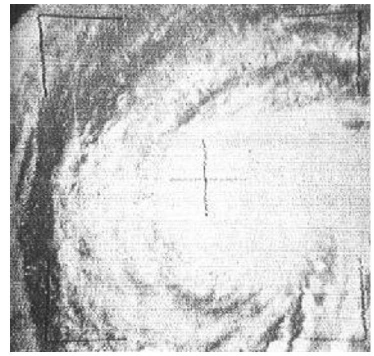

TIROS III image of Esther as a major hurricane.

It has now become possible to deduce the strength of the hurricane winds from the degree of organization seen in satellite pictures.

By the late 1960s, polar orbiting satellites with visible (VIS) and limited infrared (IR) capabilities were providing TC forecasters with coarse-resolution imagery several times a day. At this time there were no enhancement or animation capabilities. Early work by Fett (1966), Fritz et al. (1966), and Hubert and Timchalk (1969) was generally unsuccessful in inferring TC intensity from this type of imagery. As the number of satellites increased and their capabilities improved, another effort was made to use satellite imagery to determine the intensity of tropical cyclones. Working at his Washington, D.C. office at the Synoptic Analysis Branch of the Environmental Science Services Administration (ESSA – the precursor to NOAA), scientist Vernon Dvorak (Fig. Dvorak) developed his cloud pattern recognition technique based on a revolutionary conceptual model of TC development and decay. Dvorak and his colleagues derived an empirical method relating TC cloud structures to tropical cyclone intensity. The earliest internal NOAA reference to this work is Dvorak (1972), followed by an update (Dvorak 1973). Both of these technical memorandums focused on providing forecasters with a straightforward and logical methodology immediately suited for operational use. Typhoon forecasters at the JTWC, Guam, (including Chip Guard, Ed Fukada and Frank Wells) immediately put the techniques to use, and provided useful feedback. Dvorak's 1975 paper in Monthly Weather Review provided exposure of his work to the wider meteorological community (Dvorak, 1975). Throughout the 1970s and early 1980s, the pace of improvements to meteorological satellites quickened; more satellites were put in orbit, more types of satellites were developed, image resolution improved, new wavelengths of observation were added and the timeliness of the imagery increased from a few images per day to at least one image per hour.

Vernon Dvorak circa late 1970s.

An important development in the mid to late 1970s was the geostationary meteorological satellite. Appearing first over the Atlantic with the launch of GOES-1 on October 16, 1975, the first geostationary satellite in orbit over the western Pacific was on-station in 1979.

Geostationary satellites provided full earth disk VIS (daytime) and IR (day and night) pictures every hour. Whereas Dvorak's early work was applied to VIS imagery from polar orbiting satellites, a widely used technical report (Dvorak 1984) expanded Dvorak's techniques into the

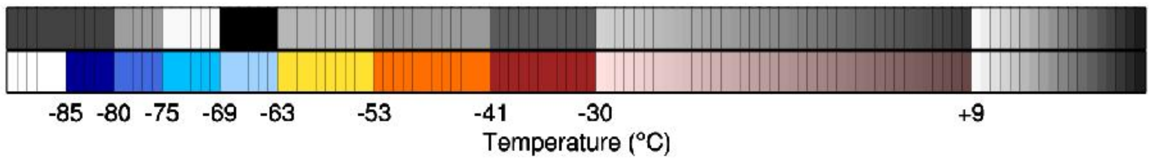

realm of infrared imagery with a special gray-shade enhancement. Dvorak developed his own false-gray-shade enhancement – the "BD" curve – for using his techniques on IR imagery (Fig. BD1). The National Hurricane Center, Miami, is experimenting with a color version of the BD enhancement. The application of these enhancements to the IR image of a real tropical cyclone is shown in Fig BD2.

Figure BD1. The equivalent IR temperature range for Dvorak's false gray shade enhancements to IR imagery – the BD curve (upper bar) and NHC's experimental color version of the BD curve (lower bar).

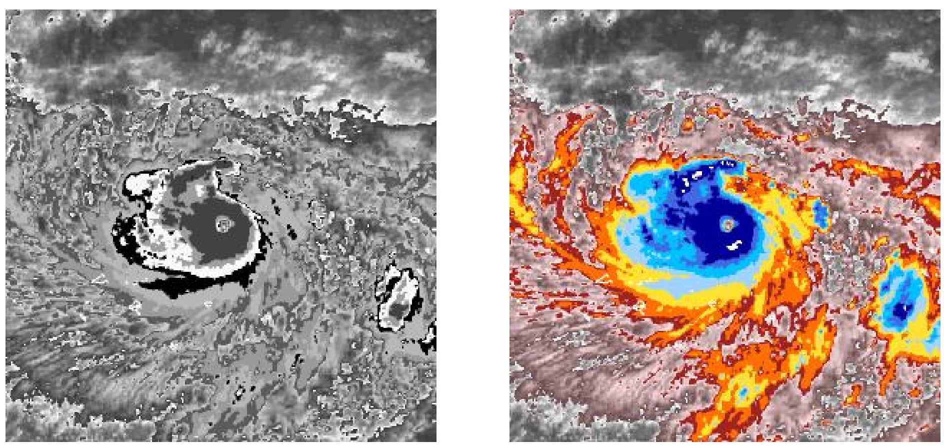

Figure BD2. Dvorak's BD enhancement curve applied to the image of Typhoon Gay (1992) (left), compared to the experimental NHC BD color enhancement curve (right).

The Dvorak techniques allow an analyst to determine the intensity of a tropical cyclone from its appearance on satellite imagery. The T number (T for Tropical) obtained from application of the techniques is analogous to a Richter scale for earthquakes in so far as the T numbers range from T 0 (T zero) to T 8.0 (T eight point zero), with T 0 being the weakest of all (i.e., < 25 kt) and T 8.0 marking the top of the scale (i.e., 170 kt). The intensities for T numbers between 0 and 8.0 distribute as follows:

T 0.5 = 25 kt		T 4.5 = 77 kt
T 1.0 = 25 kt	(TD)	T 5.0 = 90 kt
T 1.5 = 25 kt		T 5.5 = 105 kt
T 2.0 = 30 kt		T 6.0 = 110 kt

Wind speeds are 1-minute sustained

T 2.5 = 35 kt	(TS)	T 6.5 = 127 kt	(STY)
T 3.0 = 45 kt		T 7.0 = 140 kt	
T 3.5 = 55 kt		T 7.5 = 155 kt	
T 4.0 = 65 kt	(TY)	T 8.0 = 170 kt	

Characteristics of a tropical cyclone that enter the T number calculation include the degree of curvature of the primary rain band, the azimuthal extent of peripheral rain bands, the size and definition of the central cloud shield, the sharpness (in VIS imagery) and temperature (in IR imagery) of the eye, and the width (in VIS imagery) and temperature-weighted width (in IR imagery) of the eyewall cloud. These measurements taken directly from the satellite imagery yield the Data T number (DT). The DT is used in conjunction with two more T number calculations to get the Final T number (FT): (1) the Pattern T number (PT) obtained by a comparative match of the image to some much generalized stick-figure representations of classes of TCs; and (2) the Model Expected T number (MET). One of Dvorak's greatest achievements with his techniques was to establish a model for the rate of tropical cyclone intensification. He found the "typical" rate of tropical-cyclone intensification to be +1 T number per day. Some TCs intensify slower than this; others faster than this. Dvorak defined a "slow" rate of intensification as +0.5 T number per day, and a "rapid" rate of intensification as +1.5 T number per day. Of course, some tropical cyclones remain steady or begin to weaken; while others intensify at a rate that is even faster than his "rapid" rate. The analyst must carefully determine the rate at which a TC is thought to be developing, as this provides the forecast of the anticipated intensity in 24 hours. The anticipated 24-hour intensity is known as the Model Expected T Number (MET). For example, if the cyclone in question is today at T 3.0 (a 45 kt tropical storm), then it will be at T 4.0 (a minimal 65 kt typhoon) at the same time tomorrow for a typical rate of intensification. The MET for the same TC is T 4.5 (77 kt) for a "rapid" rate, and T 3.5 (55 kt – but still a tropical storm) for a "slow" rate. The MET is a powerful constraint in Dvorak's techniques to which any given determination of the PT and FT must conform. Occasionally, however, a TC really does undergo "explosive" deepening, and the DT far outpaces the MET. In such cases, the analyst may choose to "break model constraints" and let the FT be outside the bounds established by the MET.

The National Hurricane Center, Miami, has the luxury of dedicated reconnaissance aircraft support for the diagnosis of hurricane intensity. The "Hurricane Hunter" WC-130 planes are based at Keesler Air Base, Mississippi, and are tasked by the NHC for flights in the Atlantic and Gulf of Mexico. For the NHC, the Dvorak techniques provide a useful back-up when aircraft are not present or are unavailable and provide an important second opinion when both are available. From the 1950s until January 1988, the western North Pacific also had dedicated aircraft reconnaissance, with WC-130 aircraft flying out of Andersen Air Force Base, Guam. The planes were discontinued on Guam to save the Air Force $25 million per year. With congressional and senate backing, the planes were retained for the U.S. mainland (and Hawaii upon request). Guam was not left unprepared, however, as forecasters there (e.g., at the JTWC) were at the forefront in the use of the meteorological satellite for tropical cyclone applications. In addition, Guam and all of Micronesia are in good hands: it has been shown that 50% of the maximum surface wind estimates are within 5 kt of reconnaissance aircraft measurement-aided best-track intensity estimates (Brown and Franklin 2004).

Also, in 1993, Guam was provided a state-of-the-art NEXRAD weather radar.

(8) The NEXRAD Weather Radar

In making its case for the withdrawal of dedicated aircraft support for the reconnaissance of tropical cyclones in the western North Pacific, the U.S. Air Force (providers of the WC-130 hurricane hunter aircraft and crew at a cost on Guam of $25 million per year) assured its nervous customers that satellite remote sensing techniques had advanced to the point where they could satisfactorily take over the typhoon reconnaissance mission of the hurricane hunter aircraft. This included the timely and accurate provision of tropical cyclone position, intensity, and wind distribution. In addition to satellite coverage of tropical cyclones, the U.S. Air Force availed itself of an additional typhoon safeguard: it purchased and installed on Guam (in 1993) a Next Generation (1988) Doppler Weather Surveillance Radar (WSR-88D NEXRAD). The NEXRAD protects the Andersen air field by seeing beneath the cloud shield of tropical cyclones to reveal the structure of rain bands, the location of the eye and eyewall, and uses its Doppler capability to establish the bounds of damaging and destructive winds. It was placed on military-owned land at the Radio Barrigada site on Guam (Fig. NX1). This site allowed: (1) an unobstructed view to the southeast (the direction from which most typhoons make their approach to Guam); (2) an unobstructed view of the Andersen air field; (3) a sufficient distance to keep the Andersen air field out of the roughly 2-km diameter "cone of silence" encircling the radar. The site selection had a downside: from the Radio Barrigada location, the hills to the north-northeast (i.e., Mt. Barrigada) blocked the low-elevation radar beam from seeing a slice of northern Guam and the entire chain of the CNMI from Rota through Saipan (Fig. NX2).

The familiar golf ball atop the tower at Radio Barrigada, Guam houses Guam's NEXRAD weather radar.

The NEXRAD radars incorporated a number of improvements over the radar systems previously in use. The new system provided Doppler velocity, improving tornado detection and prediction ability. It provided improved resolution and sensitivity, allowing operators to see features such as cold fronts, thunderstorm gust fronts, and mesoscale to even storm-scale features of thunderstorms that had never been visible on radar. The NEXRAD radars also provided volumetric scans of the atmosphere allowing operators to interrogate the vertical structure of storms and additionally can act as wind profilers in providing detailed wind information for several kilometres above the radar site. The radars also had a much increased range allowing detection of weather features at much greater distances from the radar site.

Weather radars "see" rain drops and other airborne hydrometeors (e.g., snow and hail). Generally, the better the target is at reflecting radio waves (i.e., more raindrops, larger hailstones, etc.), the stronger the reflected radio waves, or echo, will be. The radar sends out pulses of electro-magnetic radiation in the microwave portion of the spectrum that have wavelengths that are not so long that they pass unaffected through rain areas, and not so short that they are severely attenuated. A wavelength of 10 cm (3 GHz) is used by the NEXRAD.

A Doppler radar keeps track of the phase (shape, position, and form) of the transmitted microwaves. The velocity information is retrieved by measuring the shift in phase between a transmitted pulse and a received echo, the target's radial velocity (the movement of the target directly toward or away from the radar) can be calculated. A positive phase shift implies motion toward the radar and a negative shift suggests motion away from the radar. The phase shift effect is similar to the "Doppler shift" observed with sound waves. With the "Doppler shift", the sound pitch of an object moving toward your location is higher due to compression of sound waves. As an object moves away from your location, sound waves are stretched resulting in a lower frequency. For the Doppler radar, atmospheric objects moving inbound (toward the radar) produce a positive shift in frequency of the radar signal. Objects moving away from the radar (outbound) produce a negative shift in frequency. It is this change in frequency that allows us to "see" motion in the atmosphere. The larger the phase shift, the greater the target's radial velocity.

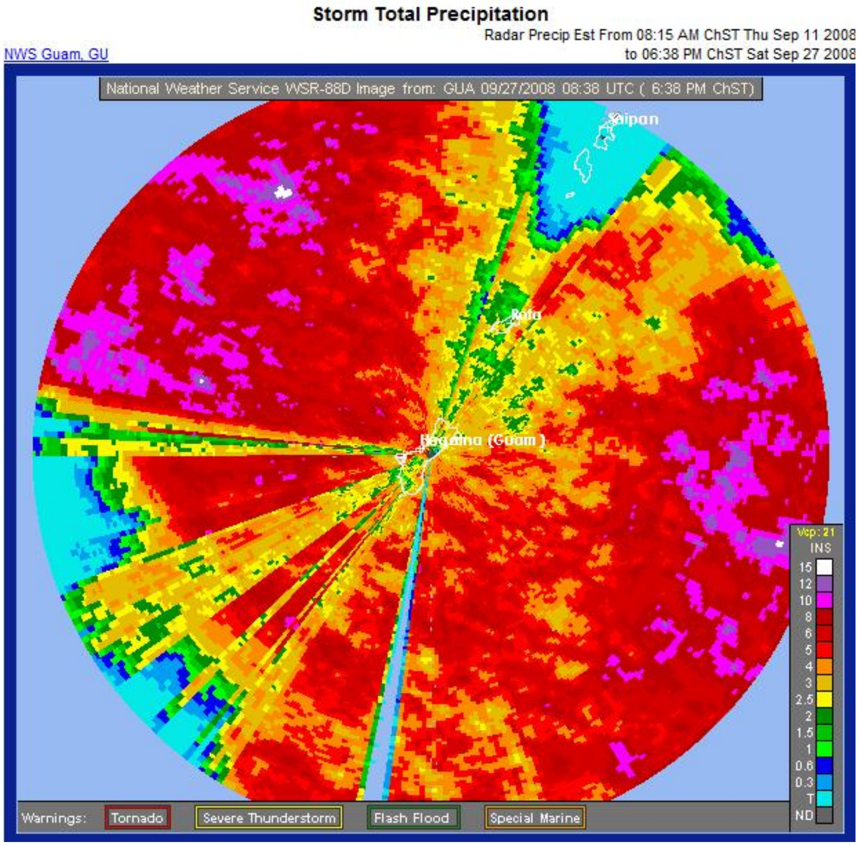

Figure NX1. An example of the Storm Total Precipitation (STP) product generated by Guam's NEXRAD. The image shows the radar-observed total rainfall over a 16-day period (11-27 September 2008). The color coding shows rainfall values in inches (e.g. pink = 10 to 12 inches). The view to the southeast and to the northwest is unobstructed. The view to the north-northeast is almost totally blocked by hills. The high terrain of the southern mountains of Guam generates a complex pattern of beam blockage to the southwest. The tiny slice of complete beam block to the south-southwest is actually an electronic artifact of the radar itself: it briefly shuts off while the beam swings past the Ladera Tower Hotel building so as not to damage the radar components by the high-intensity of reflected radar power, and (jokingly) to keep the radar beam from cooking the residents of the tower.

Another consideration for tropical cyclone applications is the change in elevation of the radar beam as distance increases from the radar site. There are three components to this: (1) a radar beam aimed roughly horizontal will refract toward the surface; (2) the beam itself is aimed at an angle above horizontal; and (3) the earth surface is curved. By beam elevation and earth's curvature only, a radar beam emitted at the lowest elevation angle departure from horizontal of 0.5° from the Guam radar site would pass 25,000 feet overhead at the location of Saipan (Fig. NX3). The curvature of the earth contributes roughly 20,000 feet to this total, and the slight upward angle of the beam itself contributing to about an additional 5,000 feet. Because of refraction, the height of the beam over Saipan will be lower than this. The amount of refraction is variable and depends on the vertical profile of atmospheric density. For a standard atmospheric density profile, a radar beam aimed horizontally would curve at a rate of 4/3 the curvature of the earth. The following equation can be used to calculate the height of the beam at any distance from the radar site:

$$H = \sqrt{r^2 + (k_e a_e)^2 + 2rk_e a_e \sin(\theta_e)} - k_e a_e + h_a\,;$$

where:
r = distance between radar and target,
k_e = 4/3,
a_e = Earth radius,
θ_e = elevation angle above the radar horizon,
h_a = height of the feed horn above ground.

Applying this equation to determine the height of the 0.5° radar beam when it reaches Saipan from Guam (220 km, or 2° of great circle arc), with a radar feed-horn elevation 100 m above sea level, the estimated height of the beam over Saipan is 4,715 m (15,469 feet).

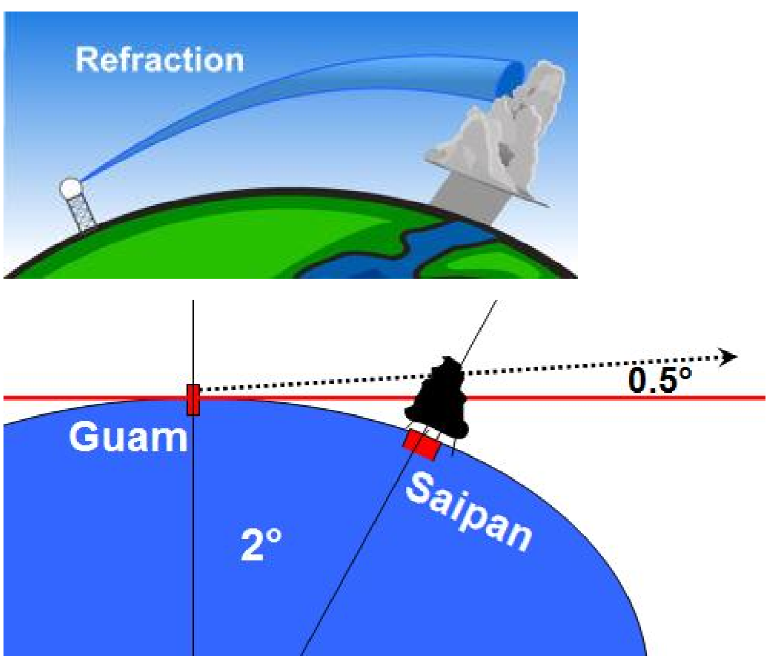

Fig. NX1. The two diagrams at left illustrate the factors contributing to the height of the radar beam as a function of the distance from the radar site. The three factors include: refraction by the atmosphere; the slight upward aim of the beam itself; and the curvature of the earth.

The structure of Soudelor was unusual. It had a tiny core embedded in a typical monsoon depression-size outer vortex (Fig.1). The eye in this tiny core is colloquially referred to as a “pin-hole” eye. It was so small that it was not resolved in microwave imagery (right panel in Fig. 1).

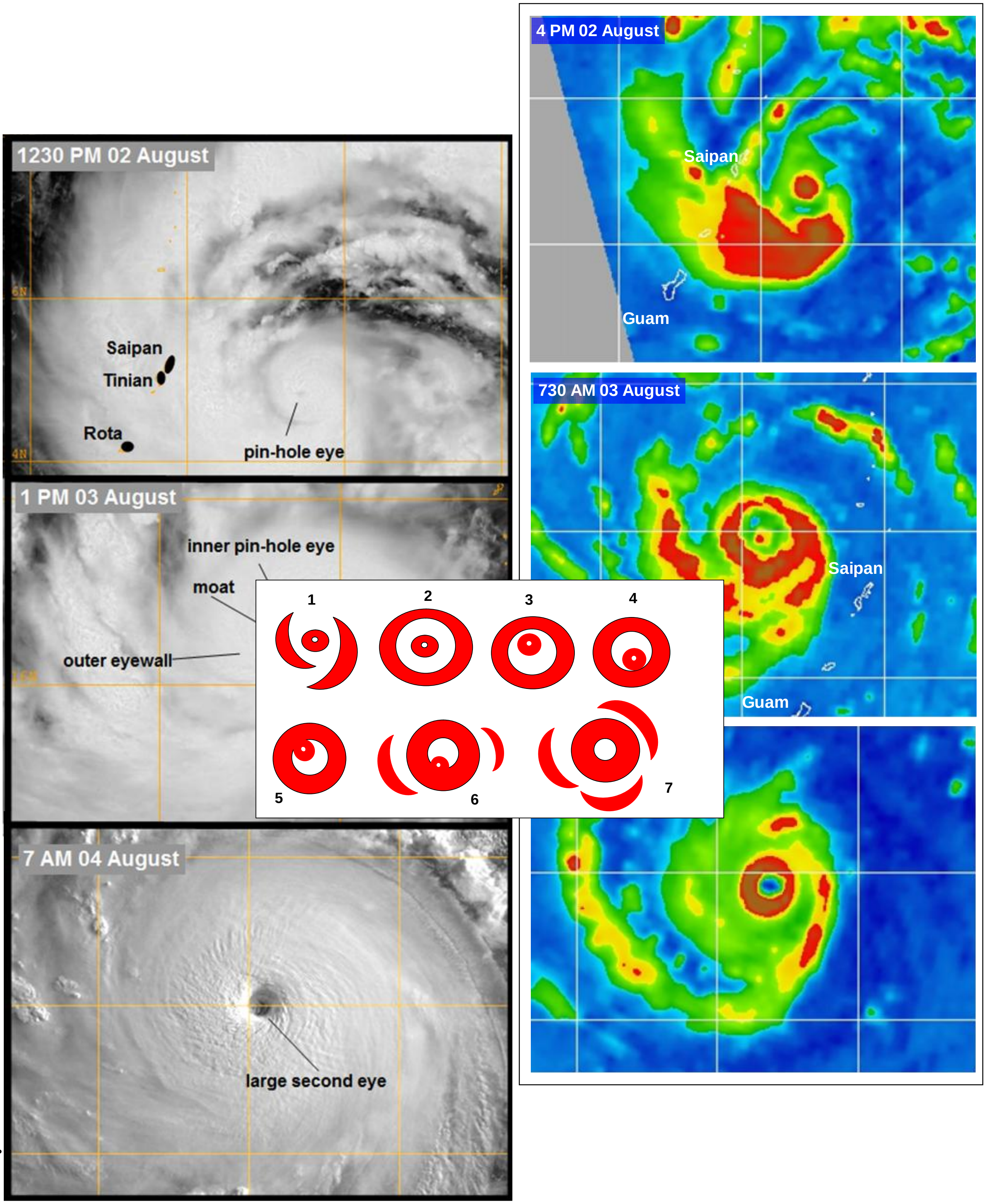

2.

2. Time line

a. Initial disturbance southwest of Hawaii
b. Formation north of monsoon trough axis
c. JTWC benchmarks
   (1) INVEST, TCFA, TD, TS, TY, STY
d. working best track
e. passage across Saipan

3. Wind Assessment

a. measured wind

There are three known direct wind measurements acquired during the passage of Soudeleor across Saipan: (1) the cup anemometer component of the ASOS system at the Saipan International Airport (SIA); (2) a cup anemometer on the grounds of the American Park; and (3) the cup anemometer component of a Davis-Pro weather station installed at a private residence on the high ground of Wireless Ridge. The anemometer at the SIA failed as the First Wind of Soudelor began its substantial rise. The last observation prior to failure was a sustained wind of 56 mph with gust to 91 mph at a time that the sea level pressure had fallen to 958 mb. It has been determined that the ASOS anemometer and other sensors did not themselves fail, but rather the communications link to the ASOS system failed as the winds increased. The anemometer at the American Park location recorded a peak gust to 87 mph (personal communication with the park ranger). A survey of the instrument site by the Saipan MET Assessment team revealed that the anemometer had been removed by the high wind (or flying debris therein) and was nowhere to be found. The 87 mph gust was thus deemed to be a floor for the wind speed, with no possible estimate from it of the actual storm peak. The third measured wind was obtained by a private resident living atop Wireless Ridge in the interior high ground of Saipan about a mile north of Capitol Hill. The instrument was a Davis Pro home weather station with a cup anemometer. The weather station was affixed to a deck on the roof of the large three-story home. The peak wind gust of 214 mph was stored in the DavisPro memory as the peak gust for the day. The owner did not personally witness this gust. He did, however, witness several gusts into the 140s to near 150 mph as he glanced at the system display during the storm. A survey of the site by the S-MET A team revealed that the instrument was still intact and functional. The large residence was in a well-exposed area at the top of the ridge with a nearly complete and open 360-degree view. The team dismissed the 214 mph gust as unreliable because the damage to structures and vegetation in the area was not severe enough for such a wind speed: trees and utility poles in the area were standing, palm trees lining the long driveway leading to the residence were in relatively good shape, the damage was less severe in this area than at many other locations on the island, and lastly, the DavisPro station was in good condition sitting in its high exposed location. The MET team did, however, accept the real-time observed gusts in the 140 to 150 mph range as plausible, and consistent with the damage at the site.

b. wind estimate by other means

There are several other ways to gain an estimate of the peak winds during Soudelor's passage over Saipan: (1) sea level pressure measurements; (2) available weather radar and meteorological satellite data; and, (3) the damage to structures, infrastructure and vegetation. By meshing observations and theory, it is possible to progressively whittle down the likely maximum winds to a narrow range, and to propose a single value as the most likely maximum 1-minute average, 10-meter height wind speed as the typhoon traversed Saipan.

The techniques used to evaluate the wind observations are those described in: Powell and Houston (1996a, b); Houston, Forbes, and Chiu (1999, 2002); and, Guard and Lander (1999). Techniques of Fujita (1971, 1992) were used to assess anomalous hurricane transients and tornados, and to determine *first wind* and *second wind* contributions. Because of the differing gust factors over land and water, the maximum sustained wind over land will be referred to as the over-water equivalent (OWE) value. This OWE is associated with a discrete gust as provided in warnings by the Joint Typhoon Warning Center. All winds are converted to 1-minute average, 10-meter elevation. Two-minute winds were converted to 1-minute winds using a conversion factor from Krayer and Marshall (1992): $w_{1min}=1.08\ w_{2min}$. Conversion to 10-meter height (when necessary) was accomplished using a logarithmic wind profile (Holton 1992). Knots were converted to miles-per-hour (mph) using the factor: $w_{mph}=1.15\ w_{kts}$.

1). Pressure: Four sea level pressure readings were acquired during Soudelor's passage over Saipan: (1) the ASOS reading of 958 mb at the time of communications failure, 938 mb at the War Memorial, 936 mb at Wireless Ridge, and 930 mb anecdotal report from a dive watch in Garapan.

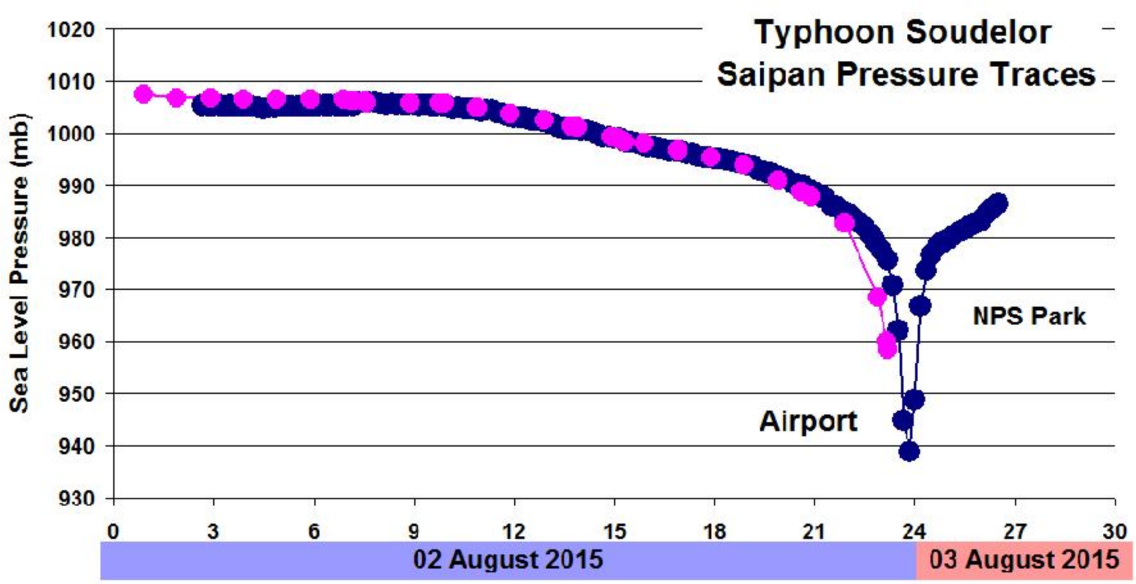

REFERENCES

Atkinson, G. D., and C. R. Holliday, 1977: Tropical cyclone minimum sea-level pressure and maximum sustained wind relationship for the western North Pacific. *Mon. Wea. Rev.*, **105**, 421-427.

Callaghan, J., and R. K. Smith, 1998: The relationship between maximum surface wind speeds and central pressure in tropical cyclones. *Australia Meteorological*, *Mag.*, **47**, 192-202.

Dickenson, M., and J. Molinari, 2002: Mixed Rossby-Gravity waves and Western Pacific tropical cyclogenesis. Part I: Synoptic Evolution, *J. Atmos. Sci*., **59**, 2183-2196.

Dvorak, V. F., 1975: Tropical cyclone intensity analysis and forecasting from satellite imagery. *Mon. Wea. Rev.*, **103**, 420-430.

Dvorak, V. F., 1984: Tropical cyclone intensity analysis using satellite data. NOAA Tech. Rep. NESDIS 11, 46 pp.

FEMA, (1993): Building Performance: Hurricane Iniki in Hawaii—Observations, Recommendations, and Technical Guidance. Federal Emergency Management Agency and Federal Insurance Administration, 100 pp.

Fujita, T. T., 1971: Proposed characterization of tornadoes and hurricanes by area and intensity. Satellite and Mesometeorology Research Project Research Paper 91, University of Chicago, 42 pp.

Fujita, T. T., 1992: The Fujita tornado scale, In "Mystery of Severe Storms", p. 31. Wind Research Laboratory Paper 239, Department of Geophysical Sciences, the University of Chicago, 298 pp.

Guard, C. P., M. P. Hamnett, C. J. Neumann, M. A. Lander, and H. G. Siegrist, Jr., 1999: Typhoon Vulnerability Study For Guam, *WERI Technical Report 85*, Water and Environmental Research Institute, University of Guam, Mangilao, Guam,156 pp.

Guard, C. P., and M. A. Lander, 1999: A Scale Relating Tropical Cyclone Wind Speed to Potential Damage for the Tropical Pacific Ocean Region: A User's Manual, *WERI Technical Report 86* (2nd edition), Water and Environmental Research Institute, University of Guam, Mangilao, Guam, 60 pp.

Holland, G. R., 1980: An analytical model of wind and pressure profiles in hurricanes. *Mon. Wea. Rev.*, **108**, 1212-1218.

Holton, J.R., 1992: The Planetary Bounday Layer. In, *An Introduction to Dynamic Meteorology*. Academic Press. New York, New York. pp 132.

Houston, S. H., G. S. Forbes, A.N.L. Chiu, 1999: The NOAA Super Typhoon Paka (1997) data acquisition team report, *Internal Report to the Working Group for Post-Storm Data Acquisition*, Office of the Federal Coordinator for Meteorological Services and Supporting Research, Silver Spring, MD, 1999.

Houston, S. H, G. S. Forbes, and A. N. L. Chiu, 2002: Impacts of Super Typhoon Paka's (1997) Winds on Guam: Meteorological and Engineering Perspectives," ASCE, *Natural Hazards Review*, **3**, pp 36-47.

JTWC, (editor F. Wells) 1991: Tropical Cyclones Affecting Guam (1671-1990). NOCC/JTWC Tech Note 91-2. US Naval Oceanography Command Center/Joint Typhoon Warning Center, Naval Oceanography Command Center, Stennis Space Center, MS. 45 pp.

Kraft, 1961: The hurricane's central pressure and highest wind. *Mariner's Weather Log*, **5**, 157.

Krayer, W. R., and R. D. Marshall, 1992: Gust factors applied to hurricane winds. *Bull. Amer. Meteor. Soc.*, **73**, 613-617.

Lander M. A., 1990: Evolution of the cloud pattern during the formation of tropical cyclone twins symmetrical with respect to the equator. *Mon. Wea. Rev.*, **118**, 1194-1202.

Lander, M. A., 1994: An exploration of the relationships between tropical storm formation in the western North Pacific and ENSO. *Mon. Wea. Rev.*, **122**, 636-651.

Lander, M. A., and C. P. Guard, 1997: High wave events: NAVSTA Family Housing Project. Prepared for Moffatt & Nichol Engineers, Long Beach, CA, 65 pp.

Marshall, T. P., 2002: Tornado damage survey at Moore, Oklahoma. *Wea. Forecasting*, **17**, 582-598.

PDN, 2003: *Pacific Daily News*, 4 Jan 2003, Gannett Publishing, pp. 1.

Powell, M. D., and S. H. Houston, 1996a: Hurricane Andrew's landfall in south Florida. Part I: Standardizing measurements for documentation of surface wind fields. *Wea. Forecasting,* **11,** 304-328.

Powell, M. D., and S. H. Houston, 1996b: Hurricane Andrew's landfall in south Florida. Part II:Surface wind fields and potential real-time applications. *Wea. Forecasting*, **11,** 329-349.

Saffir, H. S., (1972): Evaluation of structural damage caused by hurricanes. Phase 1, Final Report. National Science Foundation, Washington, D. C.

Simpson, R. H., 1974: The hurricane disaster potential scale. *Weatherwise*, **27**, 169-186.

Stewart, S. R., and S. W. Lyons, 1996: A WSR-88D radar view of Tropical Cyclone Ed. *Wea. Forecasting*, **11**, 115-135.

Velden, C. S., T. L. Olander, and R. M. Zehr, 1998: Development of an objective scheme to estimate tropical cyclone intensity from digital geostationary satellite infrared imagery. *Wea. Forecasting*, **13**, 172-186.

C. Typhoon wind damage Categories in 0.5 divisions based on the Saffir-Simpson Tropical Cyclone Scale (Guard and Lander 1999).

	Threshold		Threshold	
	1-min	gust	1-min	gust
Category	**knots**	**knots**	**mph**	**mph**
1.0	**64**	**78**	**74**	**90**
1.5	**74**	**90**	**85**	**104**
2.0	**83**	**101**	**96**	**117**
2.5	**90**	**109**	**104**	**126**
3.0	**96**	**117**	**111**	**135**
3.5	**105**	**128**	**121**	**148**
4.0	**114**	**139**	**132**	**160**
4.5	**125**	**152**	**144**	**175**
5.0	**136**	**166**	**157**	**192**

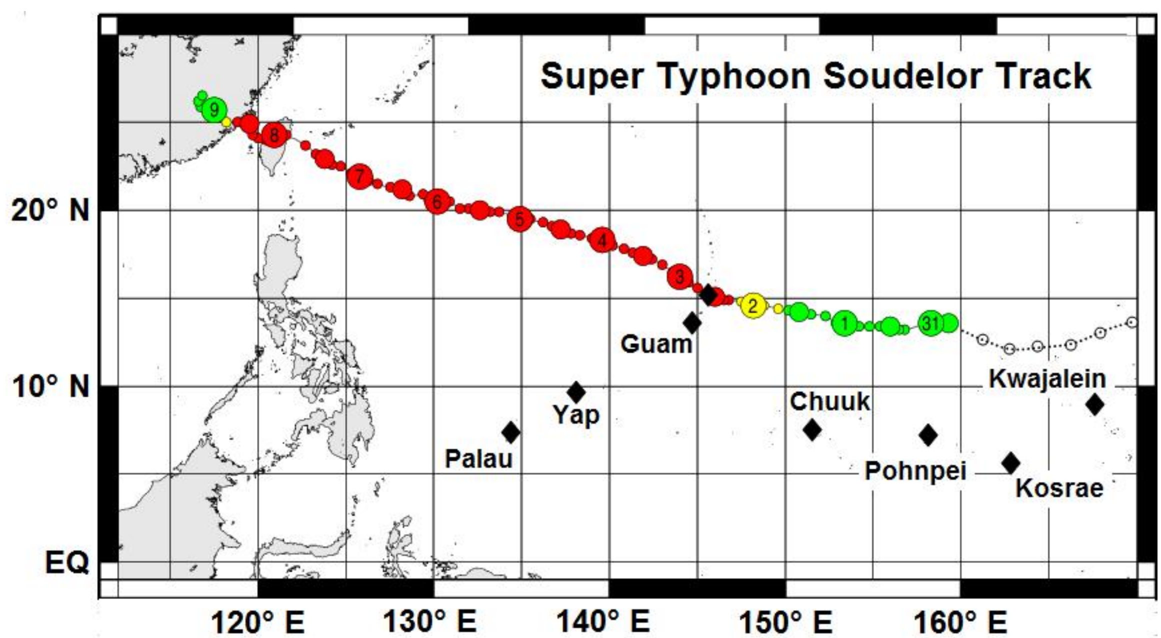

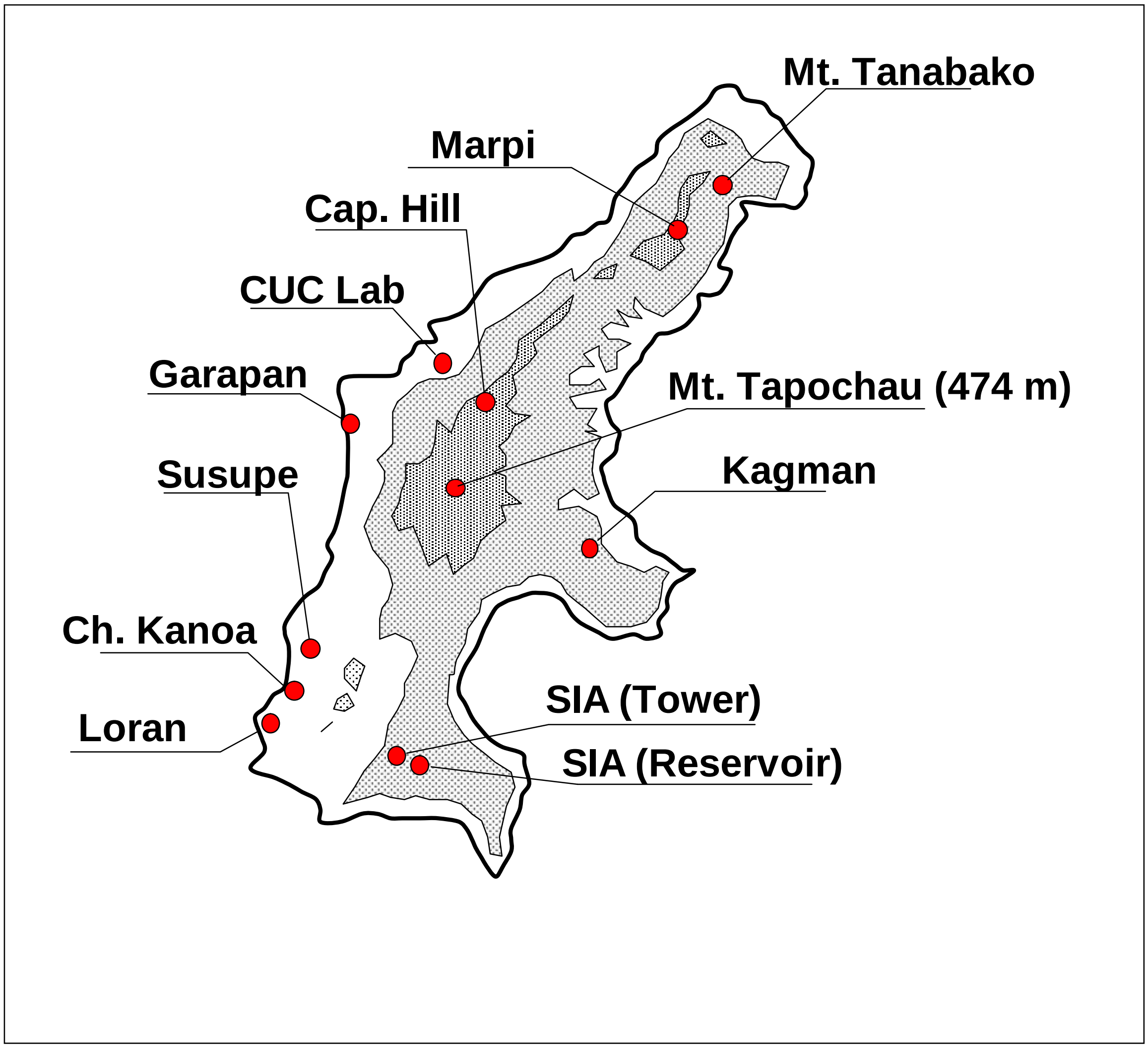
Mt. Tanabako
Marpi
Cap. Hill
CUC Lab
Garapan
Mt. Tapochau (474 m)
Susupe
Kagman
Ch. Kanoa
Loran
SIA (Tower)
SIA (Reservoir)

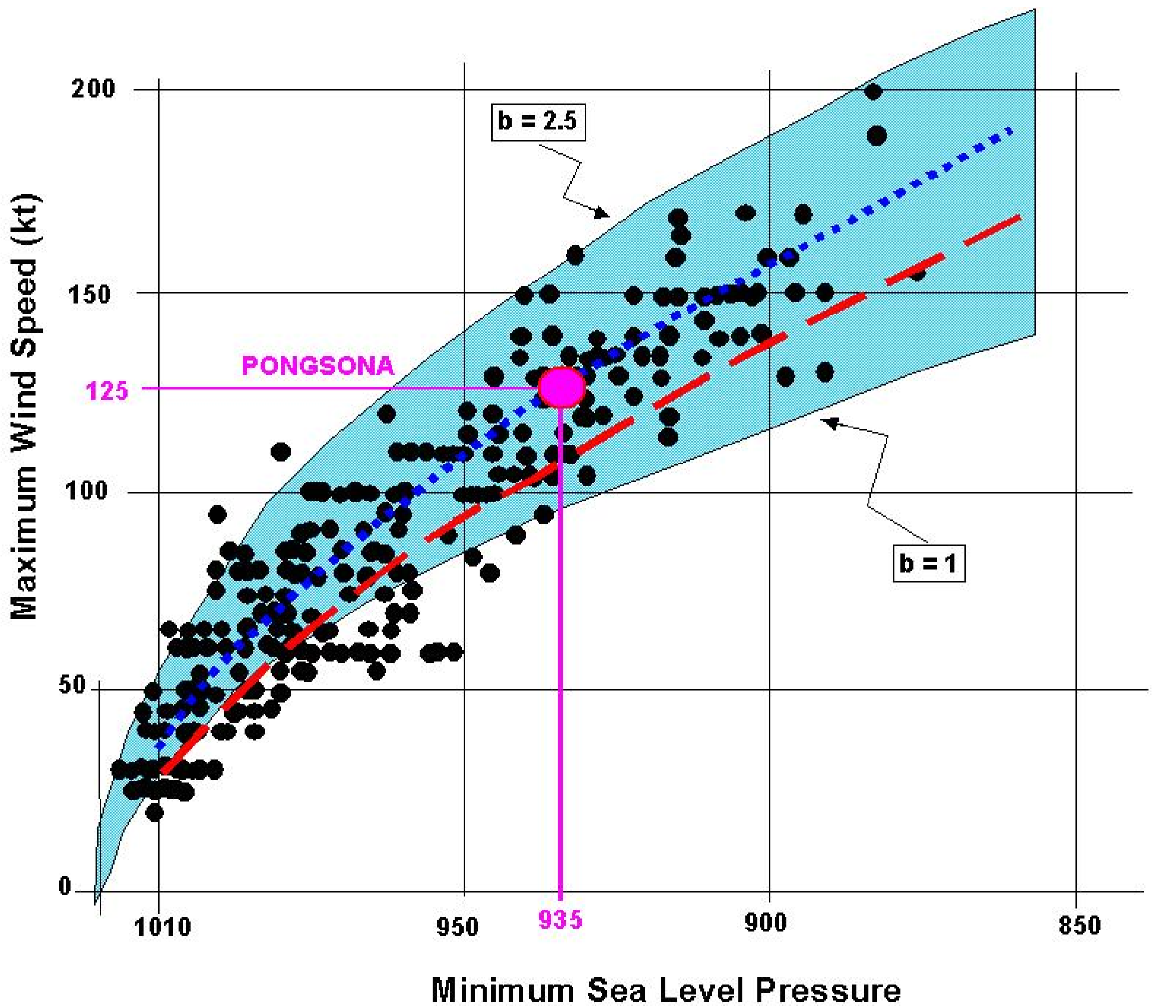

Figure 5. Relationship between maximum sustained wind and minimum sea-level pressure, where "b" values indicate theoretical limits of the relationship. Dots are actual aircraft reports for 1960's and 1970's prior to JTWC's use of the Atkinson-Holliday wind-pressure relationship (dashed line). Dotted line is the best-fit solution, and is similar to the Kraft wind-pressure relationship used in the Atlantic.

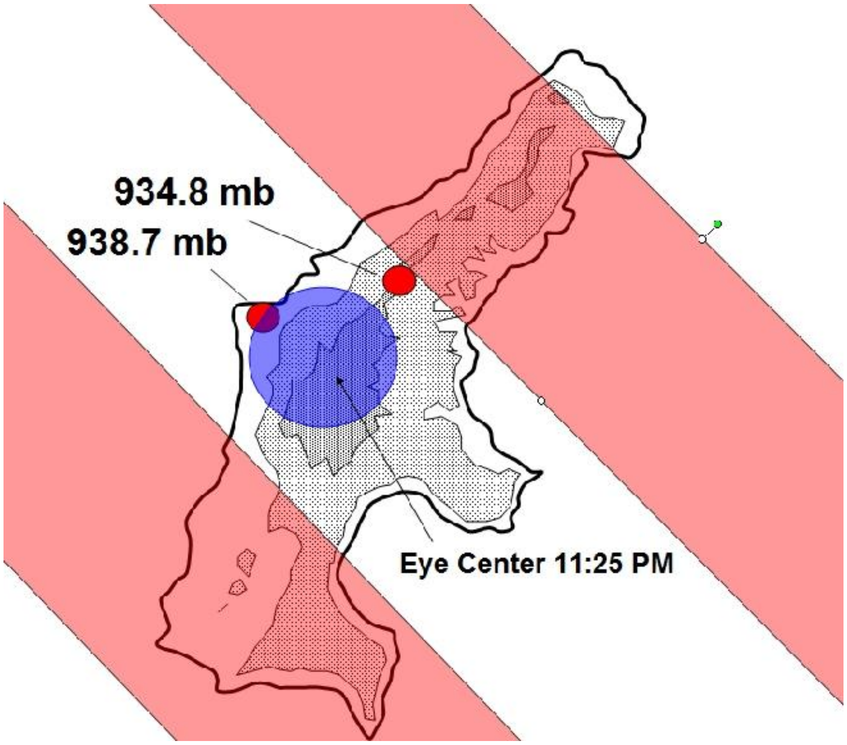

Figure 7. Track of Typhoon Soudelor's eye across Saipan.

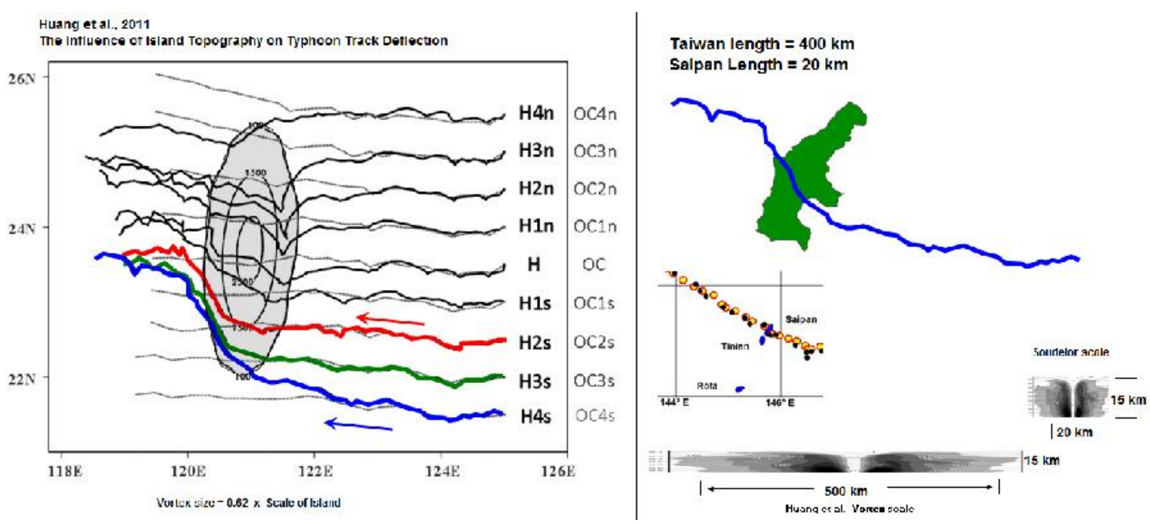

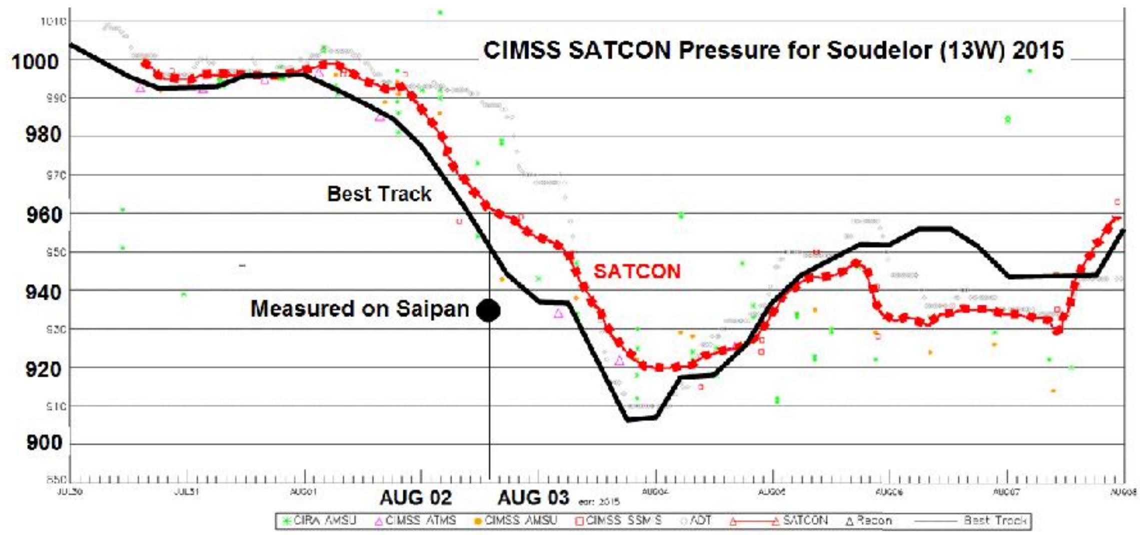

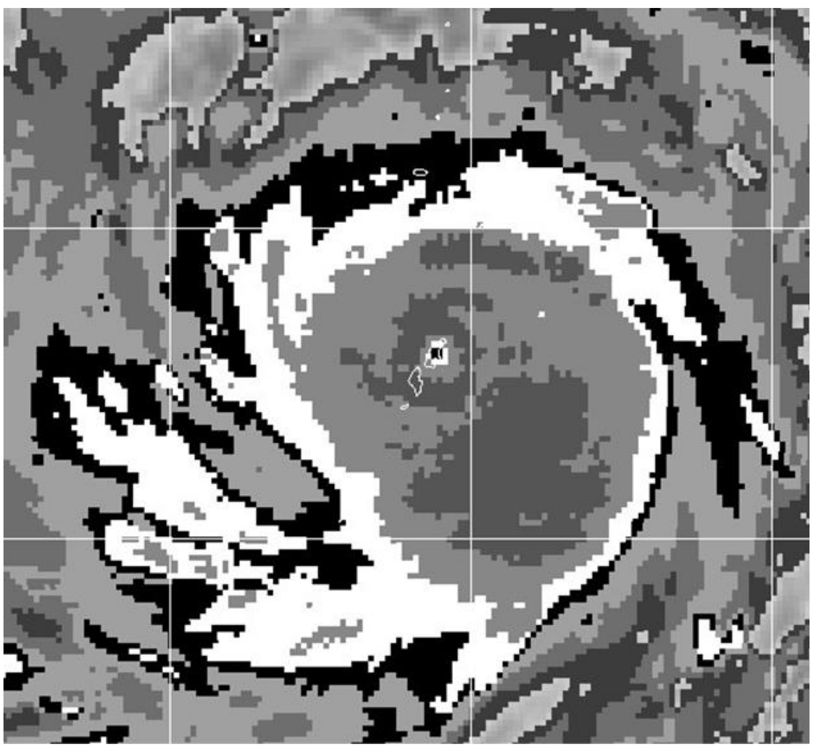

Enhanced IR (BD Curve)
1301 UTC 02 August 2015

Dvorak Analysis **Ring = CMG = T6.5**
Eye Adjust B inside CMG = -0.5
Data T Number = T 6.0

Figure 22. Roof damage.

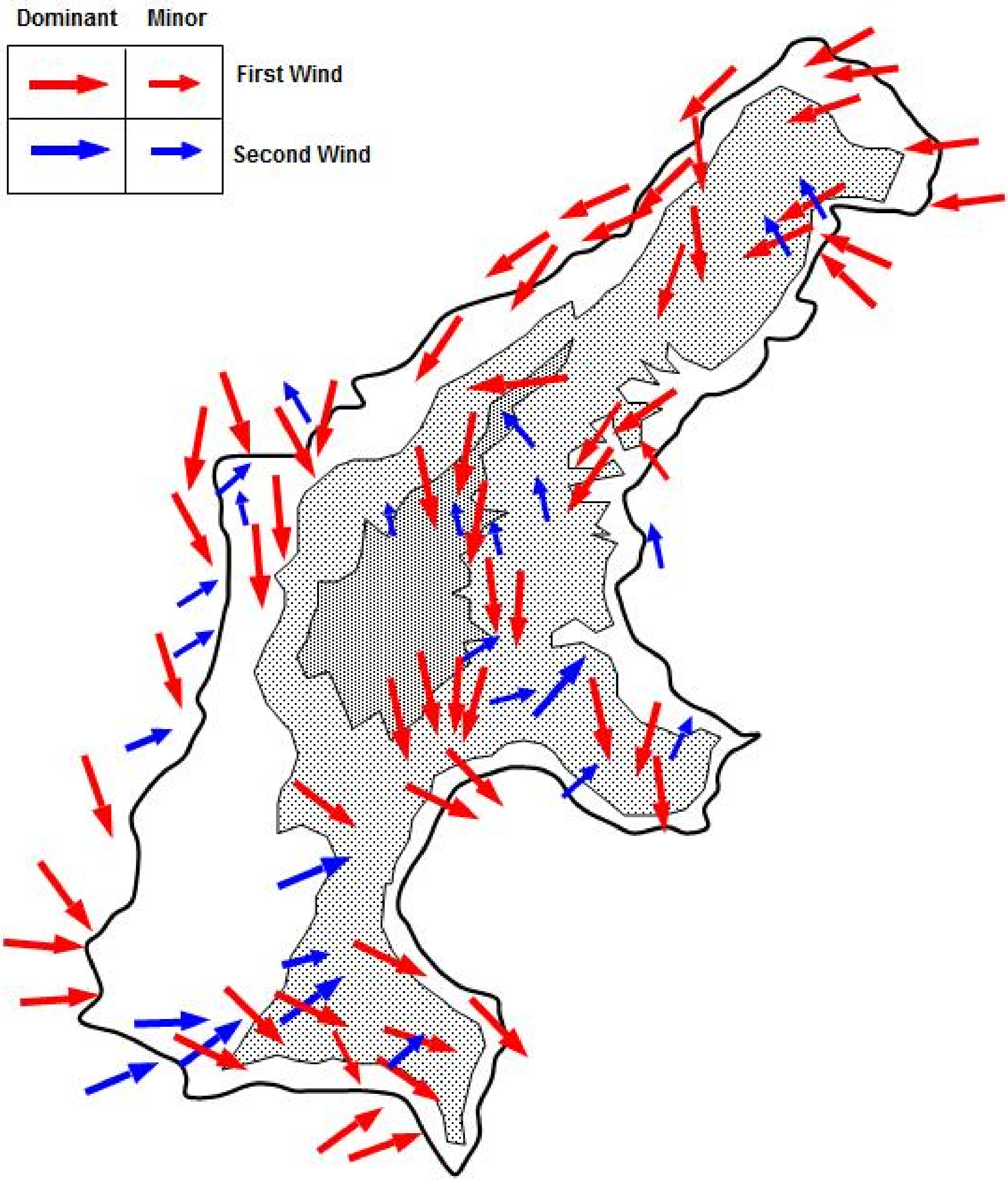

Figure 28. Analysis of tree falls that occurred during Typhoon Soudelor. Red arrows depict the “first wind” and blue arrows depict the “second wind”. The size of the arrows indicates the relative contribution of each wind component.

Figure 33.